LONG CYCLE LIFE RECHARGEABLE LITHIUM BATTERIES

FINAL REPORT

Contract No. NAS7-1100

April 23, 1990 - October 20, 1992

D. M. Pasquariello, E. B. Willstaedt and K. M. Abraham

EIC Laboratories, Inc.
111 Downey Street
Norwood, Massachusetts 02062

Submitted to

National Aeronautics and Space Administration
Jet Propulsion Laboratory
4800 Oak Grove Drive
Pasadena, California 91109

October 19, 1992

TABLE OF CONTENTS

LIST OF ILLUSTRATIONS

LIST OF TABLES

1.0 INTRODUCTION

The goal of this project was the fabrication of safe, long cycle life rechargeable Li batteries. A major hindrance to the increase of Li battery cycle life has been the highly reactive nature of the Li anode; i.e., the inefficient stripping of the plated Li on the anode due to side reactions with the solvent and electrolyte salt. Alloys of Li and Al which are rich in Li are designated δ-LiAl, and have been identified as a highly desirable novel class of anode materials for secondary Li batteries (1). During the exploratory study (1) associated with this project, the discharge and cycling behavior of δ-LiAl/TiS$_2$ cells in which the δ-LiAl composition was 90 weight-percent (w/o) Li, 85 w/o Li, or 80 w/o Li with the balance consisting of Al, were studied. (For ease of discussion the alloys will be designated 90 LiAl, 85 LiAl, and 80 LiAl, etc.) In each case, the alloy was characterized as a mixture of two phases, one being Li metal, and the other being the Li rich alloy with composition Al$_4$Li$_9$.

Preliminary studies we performed with δ-LiAl/TiS$_2$ cells containing tetrahydrofuran (THF)/1.5M LiAsF$_6$, a highly reactive electrolyte in Li anode cells, demonstrated the following:

- the alloys can be used as dimensionally stable anodes for secondary Li batteries,

- the alloy anodes in this electrolyte are less passivated than elemental Li,

- compared with cells containing elemental Li anodes, more than twice as many cycles were obtained from cells utilizing δ-LiAl anodes. The cells were cycled at 1 mA/cm^2 with a capacity for Li plating and stripping of 7 mAh/cm^2,

- the rate capability of the alloy anodes appears to be of the same order as that of Li metal anodes,

- of the three alloy anodes, 90 LiAl and 85 LiAl performed similarly and 80 LiAl worked nearly as well.

EIC's Standard Electrolyte is 48 v/o THF:48 v/o 2-Methyltetrahydrofuran (2-MeTHF):4 v/o 2-Methylfuran (2-MeF)/1.5M LiAsF$_6$. In preliminary studies (1) under cycling conditions of 1 mA/cm^2 and Li utilization of 7 mAh/cm^2, δ-LiAl/TiS$_2$ cells containing this electrolyte yielded 80 to 100 cycles. This is equal to or better than the results obtained under identical conditions in which pure Li was used as the anode. The preliminary data suggested that optimized δ-LiAl/TiS$_2$ cells would have specific energies exceeding 100 Wh/kg, volumetric energy densities greater than 250 Wh/l, and a cycle life greater than 500 deep discharge/charge cycles. In addition to the long cycle life, an expected advantage of the δ-LiAl anode cells is increased safety as a result of the reduction in the amount of elemental Li in the cell.

Several topics have been addressed in the course of the work described in this report, and the focus of all of them has been the development of a safer secondary Li cell. These topics have included the following.

- *Efficiency:* Li cycling efficiency was evaluated in $LiAl/TiS_2$ cells containing 48 v/o THF:48 v/o 2-MeTHF:4 v/o 2-MeF/$LiAsF_6$ (1.5M), 48 v/o 2-MeTHF:28 v/o Dioxolane:20 v/o THF:4 v/o 2-MeF/$LiAsF_6$ (1.5M), or 35 v/o PC:35 v/o EC:30 v/o Triglyme/$LiAsF_6$ (1.0M) as the electrolyte.

- *Safety:* A series of cells containing these electrolytes were subjected to aggressive safety studies. These tests involved heating (which we have found to produce behavior which approximates closely the effect of a thermal 'run-away' initiated by a soft short), and direct shorting.

- *Thermodynamics:* Differential Scanning Calorimetry (DSC) was used as a tool to understand the behavior and roles of the various cell components in the evolution and absorption of heat by cells containing Li or δ-LiAl anodes.

- *Carbon Anodes:* Li cycling efficiency in Li/C cells containing either petroleum coke or graphite as the carbon electrode was examined. Petroleum coke from several different industrial sources were used, and the effect of different particle size on the capacity and reversibility of the Li insertion in this type of carbon was also investigated. Graphite samples were obtained from several natural and industrial sources. The effect of several graphite carbon cleaning procedures on Li cycling performance was also investigated. This aspect of the research is a result of recent focus on the use of carbon anodes for cells with cathodes such as $LiCoO_2$ or $LiNiO_2$. Such cells are activated by charging, and Li capacity is equivalent to the initial Li content of the cathode material. Carbons used for this application therefore need to have a maximum capacity (theoretical specific capacity is 1 Li/C_6) and high Li cycling efficiency.

- *Electrolyte Salt:* Safety concerns also make it desirable to avoid the use of arsenic in the electrolyte. For this purpose the Li cycling efficiency of electrolytes with the composition 48 v/o THF:48 v/o 2-MeTHF:4 v/o 2-MeF/$LiN(CF_3SO_2)_2$ (1.2M) and 35 v/o PC:35 v/o EC:30 v/o Triglyme/$LiN(CF_3SO_2)_2$ (1.0M) was also studied.

2.0 EXPERIMENTAL

2.1 Materials

Materials and vendors were as follows: Li and LiAl alloys were obtained from the Foote Mineral Co.; 2-methyltetrahydrofuran (2-MeTHF), 2-methylfuran (2-MeF), ethylene carbonate (EC), triglyme, and CaH₂, were from Aldrich; tetrahydrofuran (THF), and propylene carbonate (PC), from Burdick and Jackson; LiAsF₆ from Lithco; LiN(CF₃SO₂)₂ was obtained from the 3M corporation; the cell separator was Celgard™ grade 2400 or 3401; graphite samples were obtained from Lonza Inc.; petroleum coke was obtained from the Unocal, Conoco, and Asbury corporations.

CaH₂ and LiAsF₆ were used as-received. LiN(CF₃SO₂)₂ was dried at 150°C and 10 mtorr overnight. THF, 2-MeTHF, 2-MeF and dioxolane were distilled from CaH₂ under flowing Argon. PC was dried over 4Å molecular sieves by stirring for about one week at room temperature, and then distilled at reduced pressure. EC, a solid at room temperature, was dried by placing it over molecular sieves and maintaining the temperature at 40°C. Purification was achieved by distillation at reduced pressure. Triglyme was dried over molecular sieves, filtered, and distilled under reduced pressure from CaH₂. For all distillations, the middle 70% fraction was collected for use. Figure 1 shows the structural formulas of the solvents used for electrolyte preparation.

The carbon materials were dried at 200°C under vacuum, and some of the graphite samples were subjected to more rigorous cleaning procedures described below.
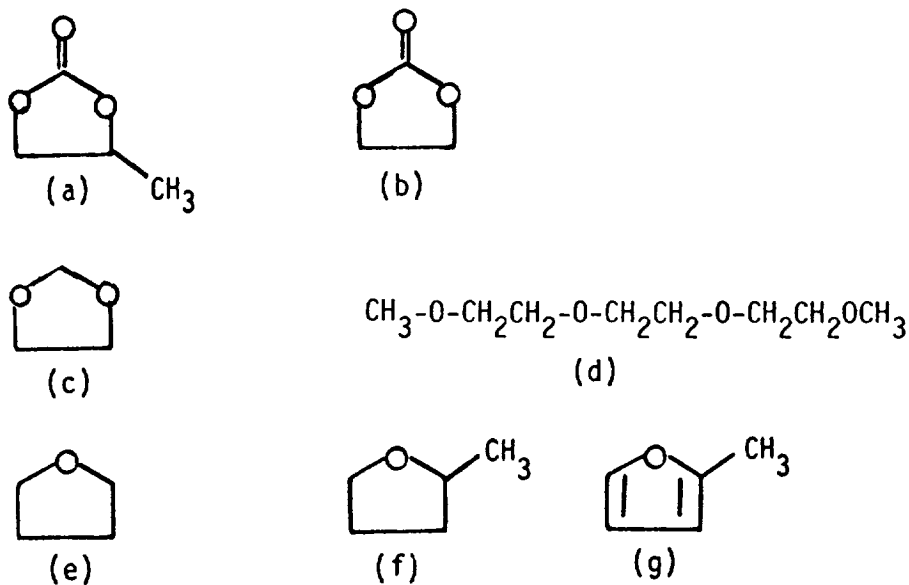
Fig. 1. Structural formulas for: (a) propylene carbonate, (b) ethylene carbonate, (c) dioxolane, (d) triglyme, (e) tetrahydrofuran, (f) 2-methyltetrahydrofuran, and (g) 2-methylfuran.

3

2.2 Electrolyte Preparation

The electrolytes containing more than one solvent were prepared by dissolving the lithium salt in the individual solvents to make a solution with the desired concentration. These solutions were then combined in specific ratios. For example, the solution containing the ether mixture and the imide salt was prepared by combining THF and 2-MeTHF solutions having a 1.2M $LiN(CF_3SO_2)_2$ concentration with 2-MeF, so that the respective volumetric ratio was 48:48:4. For solutions containing THF or a mixture of THF and 2-MeTHF where the salt was $LiAsF_6$, the solvent was cooled to -10°C prior to dissolution of the solute to minimize decomposition from the heat generated.

2.3 Materials Characterization

In order to fully characterize the anode materials, X-ray diffraction and elemental analyses were performed. To determine the elemental composition, aliquots were first hydrolyzed with water, acidified with dilute hydrochloric acid, then diluted to 10 ml. Atomic Absorption (AA) spectroscopy was used to determine the content of both metals directly. This technique yields the total metal content, and the free elemental Li content was determined by difference assuming that all the aluminum tied up an amount of lithium determined by the stoichiometry of the compound Al_4Li_9.

Scanning Electron Microscopy (SEM) was used to examine the morphology and particle size of the carbon materials.

2.4 Graphite Pre-treatment

Aliquots of Chinese flake and Madagascar natural graphites as well as Asbury A625 synthetic graphite were treated as described below.

2.4.1 Soxhlet Extraction

Approximately ten grams of each of the graphites was extracted overnight using a Soxhlet extractor and toluene. The toluene was cycled 100 times. When the extraction was complete the solid was dried under vacuum at room temperature until the pressure of the vacuum line was reduced to 20 millitorr.

2.4.2 HCl Wash

After the Soxhlet extraction was complete and the sample was dried, concentrated hydrochloric acid was added. The volume of acid used was approximately twice that of the carbon. This mixture was stirred and allowed to stand for 18 hours. At the end of this period, the solid was collected by filtration, and washed with distilled water until the filtrate showed no trace of chloride when tested with a dilute silver nitrate solution. The carbon was dried at 200°C for 18 hours under vacuum to achieve a pressure of 20 mtorr.

4

2.4.3 HNO₃ Wash

After the treatments described above were completed, the Madagascar natural graphite was extracted with concentrated nitric acid for an 18 hour period. At the end of the extraction period, the solid was filtered and washed with distilled water until the filtrate had a neutral pH. The carbon was then filtered and dried as before.

2.5 Carbon Anodes

The carbon electrodes were prepared in one of two ways. Electrodes containing graphite were made by mixing graphite (98 weight-percent (w/o)) and polyethylene (2 w/o) in decane to make a paste. This paste was spread on an expanded metal screen, cold-pressed at 1000 psi and dried at room temperature. After drying, the electrodes were pressed at 2000 psi at 140°C for two minutes. These electrodes had an average thickness of 0.025 cm (0.010 inch). Electrodes prepared using the petroleum cokes were made by suspending a mixture of 98 w/o carbon:1 w/o polyethylene:1 w/o surfactant in a hydrocarbon solvent and dipping a Ni foil substrate in the suspension. This was done several time to build up a sufficiently thick coating, and after air drying the electrode was pressed at 2000 psi for two minutes at 140°C. The average thickness of these electrodes was 0.008 cm (0.003 inch).

2.6 Li and δ-LiAl Anodes

These anodes were prepared by cutting approximately 10 cm² (3.81 cm x 2.54 cm) sections of 0.0254 cm thick foils and pressing them onto 0.0076 cm expanded Ni screen.

2.7 TiS₂ Cathodes

TiS₂ was prepared at EIC by direct combination of the elements, ground, and then sieved to a -200 mesh size. The electrodes consisted of a mixture of 97 w/o TiS₂:2 w/o surfactant:1 w/o polyethylene which was suspended in a hydrocarbon solvent, coated onto a 0.0023 cm Al foil then pressed and bonded at 140°C.

2.8 Laboratory Test Cells

Cells used were similar to those described previously (2). The electrode package was composed of one double sided cathode flanked on both sides by a Li or δ-LiAl anode, and the theoretical capacity was 60-70 mAh. The electrode package was sandwiched between two Teflon® hemi-cylinders, and inserted into a D-cell can. Compression of the electrode stack was achieved by insertion of a stainless steel shim between each hemicylinder and the wall of the can. The cover assembly consisted of a circular stainless steel plate having a stainless steel electrolyte filling tube and a Conax® fitting fixed to it. The bottom of the cover assembly has an O-ring groove, and the

cell is hermetically sealed by bolting this cover to a stainless steel ring placed at the top of the D-can compressing a Viton® rubber O-ring. Electrical connection to the electrodes are made through the Conax fitting.

2.9 AA Cells

Cathodes in the AA-size cells used for this study had a total geometric area of approximately 202 cm^2, and the theoretical cell capacity was approximately 700 mAh. Whether the anode was Li or δ-LiAl, the Li:TiS_2 ratio was between 3.4:1 and 3.9:1.

2.10 Cell Cycling Tests

Laboratory Li/TiS_2 and δ-LiAl/TiS_2 cells were mostly cycled at a current density of 1 mA/cm^2 for both discharge and charge. Both full (3 mAh/cm^2) or 25% (0.75 mAh/cm^2) depth of discharge (d.o.d.) cycling was performed. AA cells were cycled at a 100% d.o.d. (3.5 mAh/cm^2), with discharge at 1.4 mA/cm^2 and charge at 0.70 mA/cm^2. Abuse testing of AA cells consisted of shorting and heating cells which had been cycled five times. Cell voltage and temperature were recorded in both cases. For the shorting test, a 2 mΩ shunt was used to measure the current.

Experiments with carbon electrodes involved cycling Li/C cells. The cells were prepared in a manner similar to the one used for the Li/TiS_2 laboratory cells described above, and contained PC/1.0M $LiClO_4$ as the electrolyte. Cycling was performed at a constant current density of 0.1 mA/cm^2 between the limits of 2.0 and 0.1 volts. All cell data were collected using a Bascom-Turner Instruments microprocessor controlled recorder.

2.11 Differential Scanning Calorimetry

Differential Scanning Calorimetry (DSC) measurements were performed using a Perkin-Elmer DSC-7 Differential Scanning Calorimeter. Weighed aliquots were hermetically sealed in stainless steel capsules obtained from Perkin-Elmer. Baseline correction was obtained by measuring the heat flow for the calorimeter with both sample and reference chambers empty. An empty capsule was used in the reference chamber during each sample measurement. The instrument was purged with Argon throughout the experiments, and Perkin-Elmer software was used to analyze the data. The temperature range used for these experiments extended from 25°C to 290°C.

6

3.0 RESULTS AND DISCUSSION

3.1 Anode Composition

Anodes were either Li foil or δ-LiAl alloy. Lithium and aluminum combine to form several distinct phases. A solid solution containing up to 7 atomic percent (a/o) Li, is designated the α-phase. At higher Li content, the non-stoichiometric β-phase is formed, and its composition range is 46 a/o to 54 a/o Li. Both α- and β-phases coexist when the Li content is between 18 and 46 a/o. Compositions containing between 60 and 70 a/o Li belong to the γ-phase, while the δ-phase is formed for Li compositions greater than 70 a/o. In this composition, elemental Li coexists with Al_4Li_9.

The composition range of alloy which we used was 86 to 95 a/o (or 60 to 85 weight percent Li) and it is therefore classified as δ-LiAl. X-ray diffraction patterns (see Fig. 2) of the alloys showed the presence of two phases, elemental Li and Al_4Li_9. We determined the Li and Al content directly in all the anode materials using Atomic Absorption spectroscopy, and Table 1 is a summary of the results. Statistical analysis of the data results in a 95% confidence range of ±2.3% for Li and ±1.5% for Al. It was assumed that all the aluminum was bound to Li in the form of Al_4Li_9. Elemental or 'free' Li was determined from the difference between the total Li and the amount calculated to be present in Al_4Li_9.
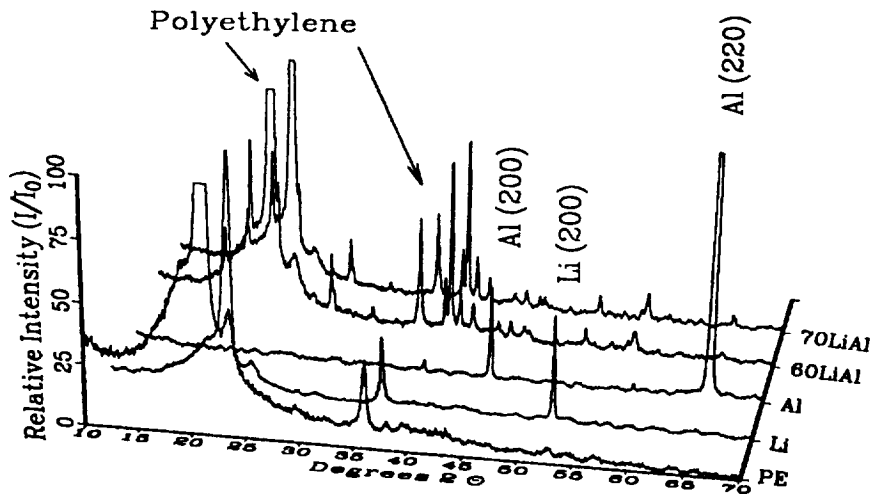
Fig. 2. X-ray diffraction patterns for polyethylene, Li, Al, 60 LiAl, and 70 LiAl.

7

Table 1. Elemental Analysis Results[a] for Several LiAl Alloys.

Nominal Anode Composition[b]	Wt. % Li Determined by AA[c]	Wt. % Al Determined by AA	Total Wt. % via AA
Li	98.6		98.6
85 LiAl	87.5	15.3	102.8
80 LiAl	83.3	22.5 (20.47)[b]	105.6
70 LiAl (#1)	67.7	29.3 (29.63)[b]	96.9
70 LiAl (#2)	72.2	29.7 (30.23)[b]	101.9
60 LiAl (#1)	60.4 (59.26)[b]	37.0 (38.57)[b]	97.4 (97.83)[b]
60 LiAl (#2)	57.9	38.4 (39.85)[b]	96.2

a) Statistical analysis indicates a 95% confidence range of ±2.3% for Li and ±1.5% for Al content determined at EIC Laboratories.
b) Value provided by the supplier.
c) AA stands for atomic absorption spectrophotometry.

3.2 Lithium Cycling Efficiency

Laboratory cells were used as a means to evaluate the Li cycling efficiency of δ-LiAl alloy anodes in three electrolytes. The FOM_{Li} value is defined by the relationship shown in equation [1].

$$FOM_{Li} = \frac{(total\ accumulated\ discharge\ capacity)}{(theoretical\ Li\ capacity)} \qquad [1]$$

FOM_{Li} is related to the Li cycling efficiency by equation (2).

$$E_{Li} = \left(1 - \frac{1}{FOM_{Li}}\right) 100 \qquad [2]$$

In the case of the δ-LiAl alloys, FOM_{Li} values may be calculated two ways. These involve using either the total Li content, or the amount of free elemental Li determined by the difference between total Li content and the amount of Li bound to Al to form Al_4Li_9. We have observed previously that the cycling efficiency of Li anodes in laboratory cells containing the standard binary electrolyte

is 96-97.5% (3), while AA Li/TiS$_2$ cells developed at EIC have demonstrated a cycle life of 250 cycles and an average Li cycling efficiency of 99.0% (4). Cycling efficiencies for cells with δ-LiAl alloy anodes and the standard electrolyte are closer to these values when FOM$_{Li}$ values determined from the 'free' Li content are used. For this reason all cycling efficiencies for the δ-LiAl/TiS$_2$ cells are calculated using FOM$_{Li}$ (free). Tables 2 through 4 are summaries for the results obtained with electrolytes having THF/2-MeTHF, 2-MeTHF/Dioxolane/THF and PC/EC/Triglyme as the principle components.

Table 2 shows the results obtained with the standard electrolyte. For the 85 LiAl anode, the cycling efficiency is higher (95.8% vs. 94.0%) when cycling is performed at the 25% d.o.d. For all other alloy anodes, the efficiency is higher when the depth of discharge is 100%. Figure 3 shows typical cycling curves obtained for the 70 LiAl/TiS$_2$ cells cycled at the two discharge depths.

The results obtained with the 2-MeTHF/Dioxolane/THF ternary electrolyte are summarized in Table 3. For each alloy used, the Li cycling efficiency is greatest when the cycling depth is restricted to 25% of the theoretical capacity. Figure 4 compares typical cycling curves for 70 LiAl/TiS$_2$ cells containing this electrolyte and cycled at the two different depths of discharge.

The results summarized in Table 4 were obtained with the PC/EC/Triglyme ternary electrolyte, and emphasize the effect of electrolyte upon the cycling efficiency. In this case the Li cycling efficiency is virtually the same at either depth of discharge when the anode is 85 LiAl. For the 80 LiAl, 70 LiAl and 60 LiAl alloy anodes, the Li cycling efficiency is higher when the discharge depth is 25%. The greatest effect of discharge depth on cycling efficiency was observed when the anode was 60 LiAl. For the 100% d.o.d. the efficiency was 94.3% while it was 96.7% at the lower discharge depth. Cycling curves obtained with 70 LiAl/TiS$_2$ cells containing this electrolyte and cycled at either 25% or 100% d.o.d. are shown in Figure 5.

We observed that the discharge capacity of cells containing the EC:PC:Triglyme ternary electrolyte gradually increased over the first several cycles, a phenomenon that may also be attributable to the gradual disruption of a passivating film on the anode. The two 70 LiAl/TiS$_2$ cells containing this electrolyte could not be cycled initially at 1 mA/cm^2. However, after five to eleven cycles at 0.25 mA/cm^2, it was possible to increase the current density to 1 mA/cm^2 for both discharge and charge.

At first, laboratory cells having a 70 LiAl anode and either PC/LiAsF$_6$ (1M) or 90 v/o PC:10 v/o 2-MeF/LiAsF$_6$ (1M) also could not be cycled at 1 mA/cm^2. On the other hand, after 11 or 12 cycles with the current density at 0.25 mA/cm^2 for both discharge and charge, it was possible to increase the discharge current density to 1 mA/cm^2. (The charge current density was maintained at 0.25 mA/cm^2). The Li cycling efficiency was 93.9% for the cell containing the PC/LiAsF$_6$ electrolyte and 94.7% for the one containing the PC:2-MeF/LiAsF$_6$ mixed electrolyte. Figure 6 shows typical cycling curves for these two cells. The need to cycle at low rate may be related to the disruption of a passivating layer at the anode surface in cells having electrolytes containing PC.

9

Table 2. Lab Cell Cycling Results in the Standard Electrolyte.*

Cell No.	Anode	Current Density (mA/cm^2)	Specific Capacity (mAh/cm^2)	No. of Cycles	Cycling Efficiency	
					FOM$_{Li}$	%
51	85 LiAl	1.0	3.0	228	16.6	94.0
20	85 LiAl	1.0	0.75	899	23.8	95.8
23	80 LiAl	1.0	3.0	347	25.2	96.0
52	80 LiAl	1.0	0.75	607	22.0	95.4
38	70 LiAl	1.0	3.0	411	27.7	96.4
63	70 LiAl	1.0	0.75	775	22.3	95.5
36	60 LiAl	1.0	3.4	276	23.4	95.7
37	60 LiAl	1.0	0.75	528	19.5	94.9

*48 v/o THF:48 v/o 2-MeTHF:4 v/o 2-MeF/LiAsF$_6$ (1.5M).

Table 3. Lab Cell Cycling Results in the 2-MeTHF/dioxolane/THF Ternary Electrolyte.*

Cell No.	Anode	Current Density (mA/cm^2)	Specific Capacity (mAh/cm^2)	No. of Cycles	Cycling Efficiency	
					FOM$_{Li}$	%
21	85 LiAl	1.0	3.0	481	21.2	95.3
22	85 LiAl	1.0	0.75	1076	27.5	96.4
25	80 LiAl	1.0	3.0	474	18.4	94.6
26	80 LiAl	1.0	0.75	809	23.1	95.7
54	70 LiAl	1.0	3.40	296	17.0	94.1
53	70 LiAl	1.0	0.80	898	24.7	96.0
58	60 LiAl	1.0	3.40	349	22.5	95.6
57	60 LiAl	1.0	0.80	945	26.0	96.2

*48 v/o 2-MeTHF:28 v/o dioxolane:20 v/o THF:4 v/o 2-MeF/LiAsF$_6$ (1.5M).

Table 4. Lab Cell Cycling Results in the PC/EC/Triglyme Ternary Electrolyte.*

Cell No.	Anode	Current Density (mA/cm^2)	Specific Capacity (mAh/cm^2)	No. of Cycles	Cycling Efficiency	
					FOM$_{Li}$	%
33	85 LiAl	1.0	3.0	513	17.7	94.4
34	85 LiAl	1.0	0.75	711	17.2	94.2
29	80 LiAl	1.0	3.0	525	16.6	94.0
30	80 LiAl	1.0	0.75	691	19.4	94.9
56	70 LiAl	1.0	3.0	457	17.1	94.2
55	70 LiAl	1.0	0.75	759	21.4	95.3
60	60 LiAl	1.0	3.0	699	17.6	94.3
59	60 LiAl	1.0	0.75	1050	30.0	96.7

*35 v/o PC:35 v/o EC:30 v/o triglyme/LiAsF$_6$ (1.0M).
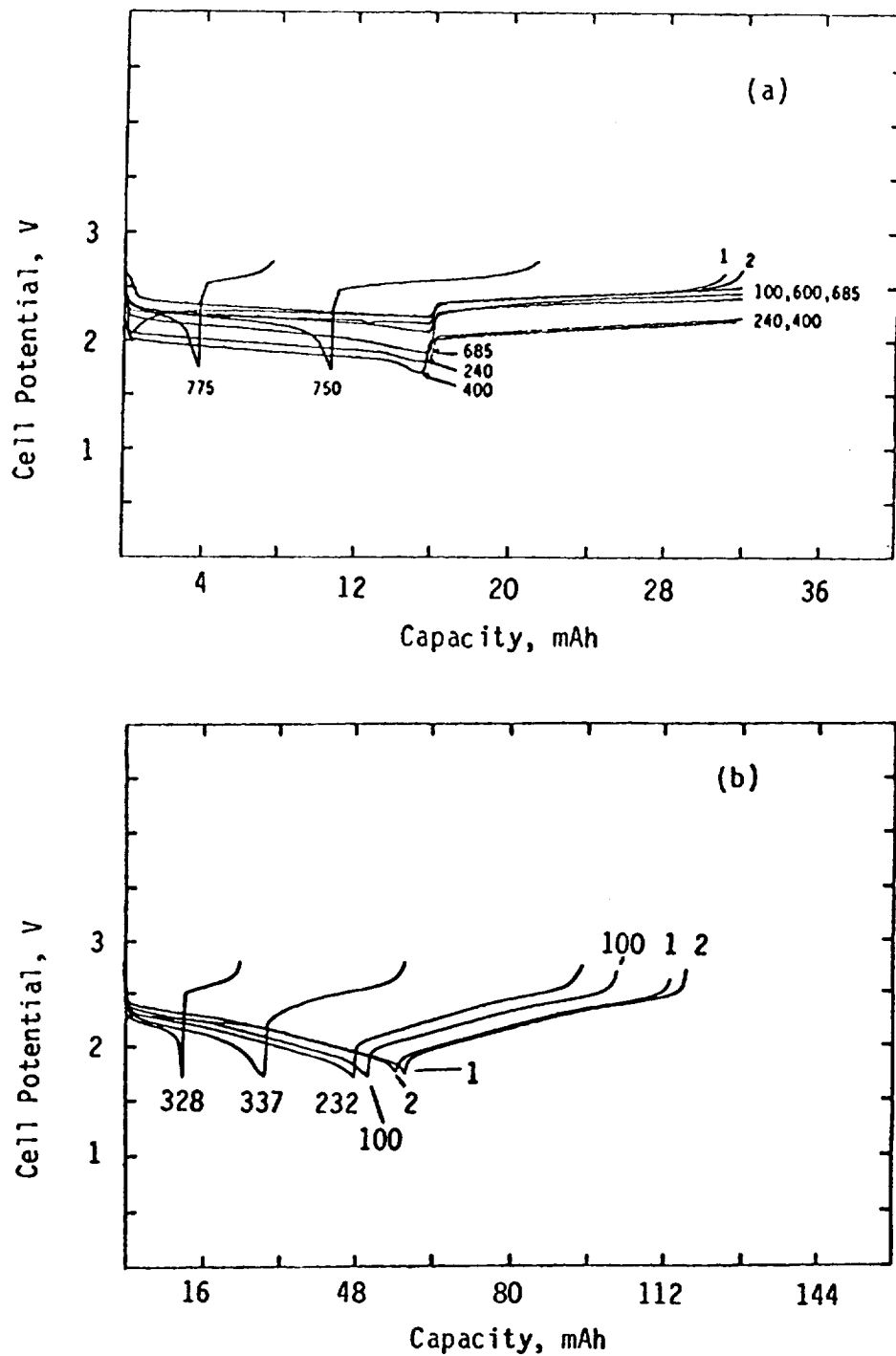
Fig. 3. Typical cycling curves at (a) 25% d.o.d. and (b) 100% d.o.d. for laboratory cells containing the standard binary electrolyte and 70 LiAl anodes. The current density has 1 mA/cm^2. Theoretical capacity was 67 mAh.

12
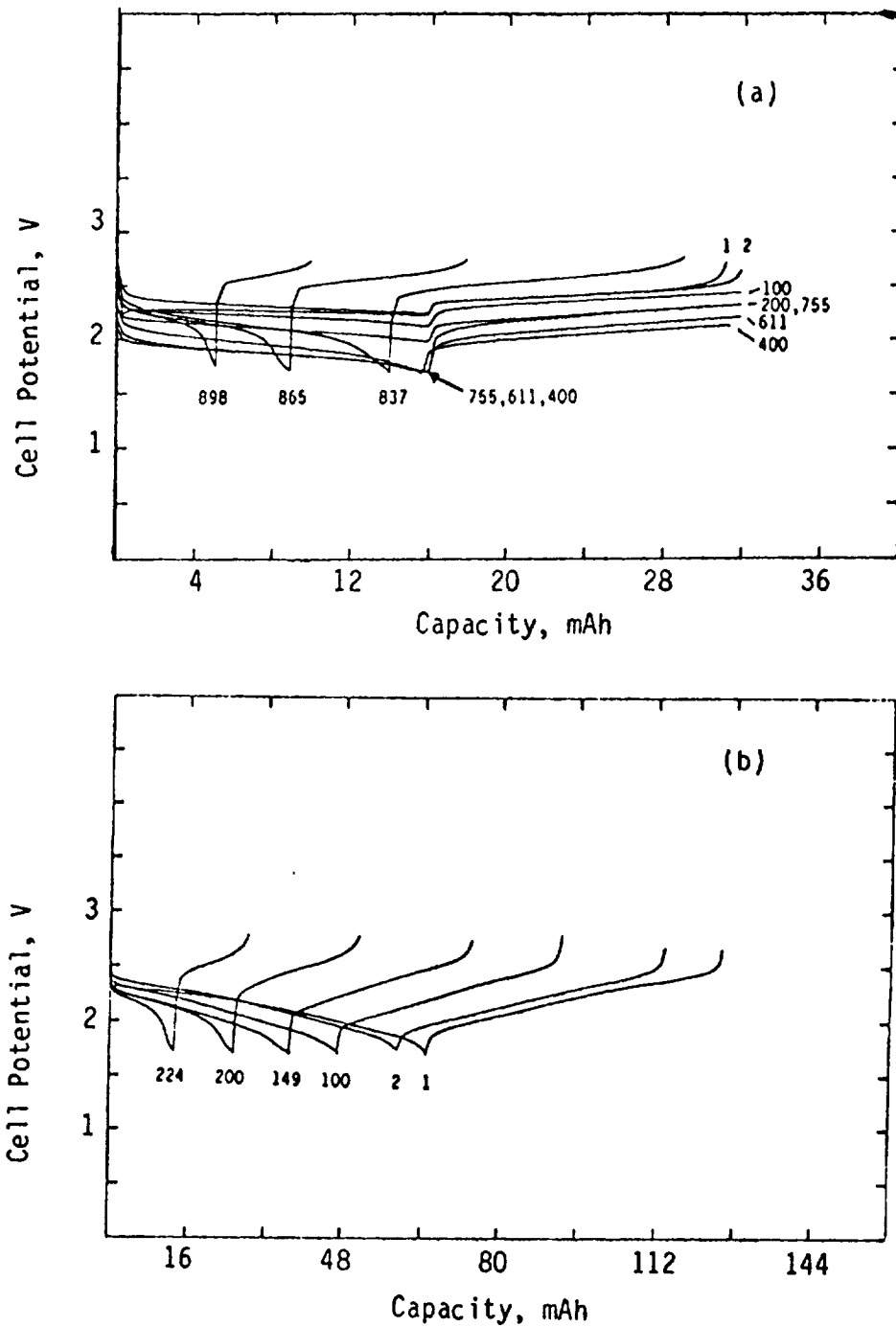
Fig. 4. Typical cycling curves at (a) 25% d.o.d. and (b) 100% d.o.d. for laboratory cells containing the dioxolane ternary electrolyte and 70 LiAl anodes. The current density was 1 mA/cm². Theoretical capacity was 67 mAh.
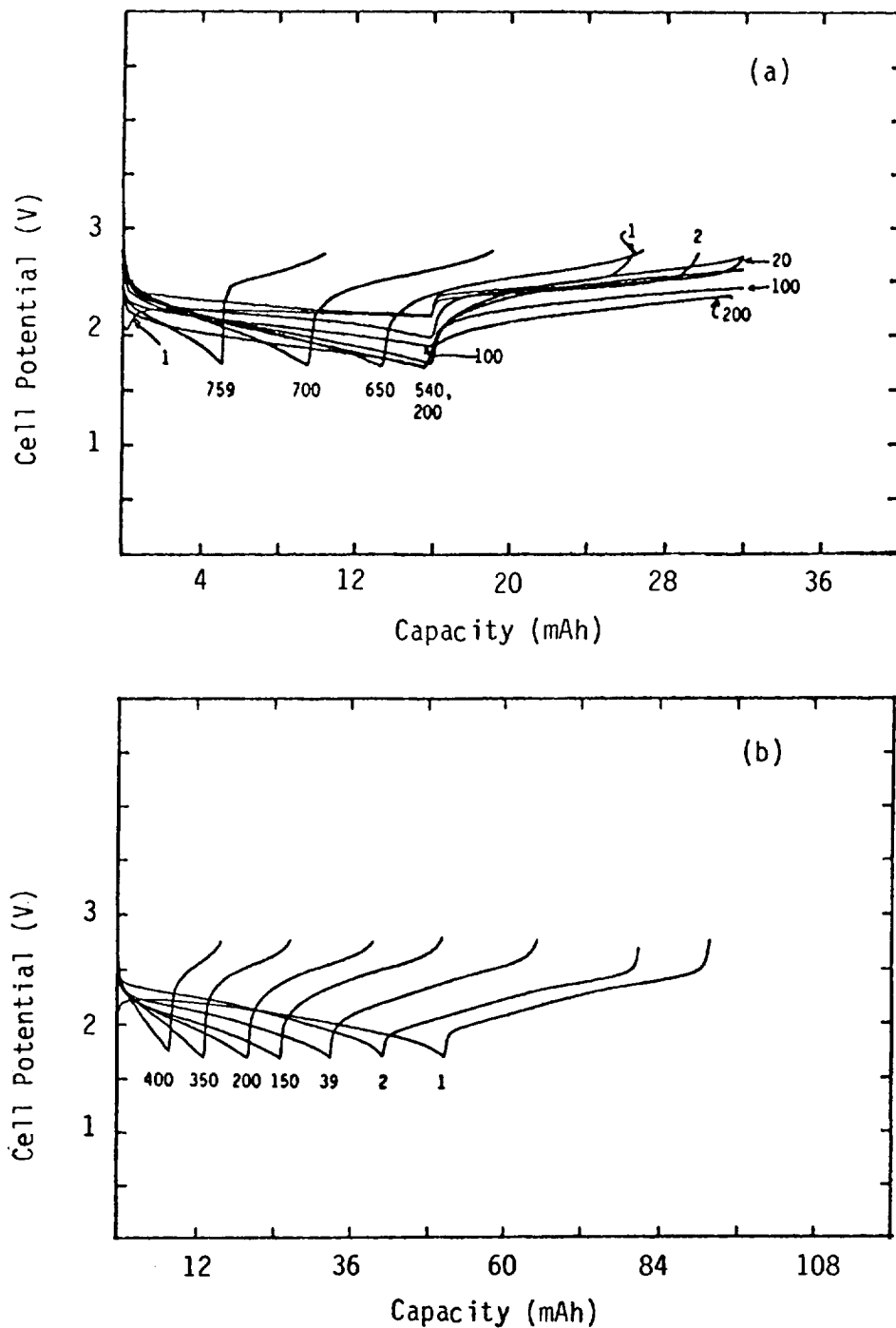
Fig. 5. Typical cycling curves at (a) 25% d.o.d. and (b) 100% d.o.d. for laboratory cells containing the triglyme ternary electrolyte and 70 LiAl anodes. The current density was 0.25 mA/cm^2 for the first 11 cycles at the 25% d.o.d. as well as the first five cycles at the 100% d.o.d. All other cycles were performed at 1 mA/cm^2 for discharge and charge. Theoretical capacity was 67 mAh.

14
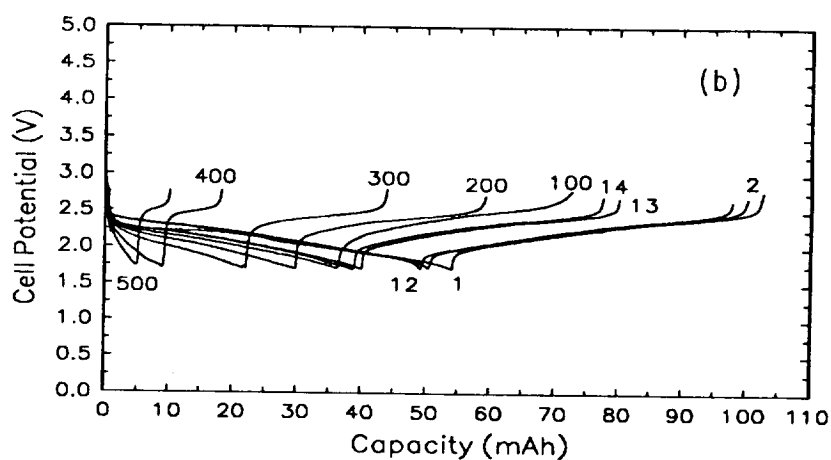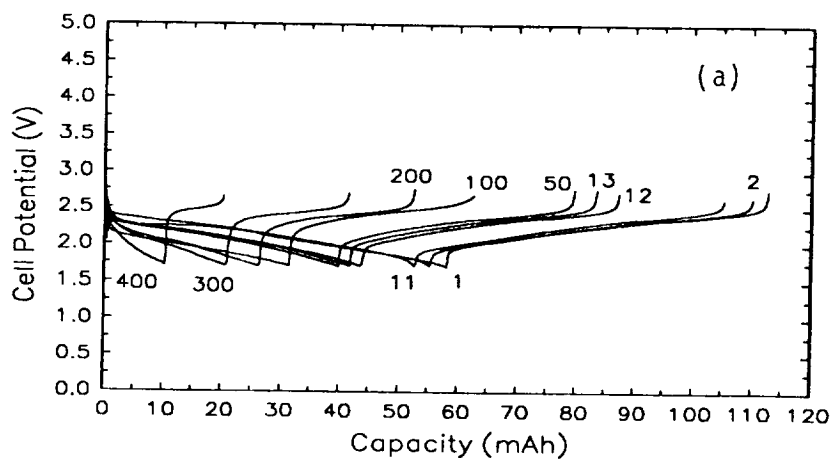
Fig. 6. Cycling curves for 70 LiAl/TiS$_2$ laboratory cells containing (a) PC/1.0M LiAsF$_6$ or (b) 90 v/o PC/10 v/o 2-MeF/1.0M LiAsF$_6$. The current density was 0.25 mA/cm^2 for both discharge and charge for the first twelve cycles in (a) and the first eleven cycles in (b). All other cycles were performed with a current density of 1 mA/cm^2 for discharge and 0.25 mA/cm^2 for charge. Theoretical capacity was 62 mAh.

It is reasonable to expect that the safest practical cell would be one developed using an anode that has the least amount of free Li. Of the materials which we tested, it is the 60 LiAl alloy that meets this criterion. Unfortunately, this alloy is not very malleable, a condition which hampers anode fabrication. The 70 LiAl is the next best choice for further testing in AA-size cells since it can more easily be shaped into a spirally wound configuration, without appearing to offer any significant Li cycling efficiency penalty.

3.3 Performance of AA Cells

3.3.1 Capacity/Rate

Cycling curves from tests performed with 70 LiAl/TiS2 cells containing the standard binary and the dioxolane ternary electrolyte are shown in Figures 7 and 8, respectively. Theoretical capacity of these cells was approximately 700 mAh. At the lowest rate (0.75 mA/cm^2) the discharge capacity was 680 mAh for both cells. At the highest (5 mA/cm^2) discharge rate, the capacity was 600 mAh for the cell containing the standard binary and 567 mAh for the one with the dioxolane ternary.

3.3.2 Cycle Life

Cycling of the cells used in the rate study was continued. For 70 LiAl/TiS$_2$ AA cells, cycled at a 100% d.o.d., the capacity was $\geq$80% of the nominal capacity for 85 cycles when the standard electrolyte was used and 60 cycles when the electrolyte was the dioxolane ternary. The cycling efficiency was 95.8% in the case of the standard electrolyte, and 94.3% for the ternary mixture containing dioxolane. It will be recalled that Li/TiS$_2$ AA cells developed at EIC (which contain the standard electrolyte) yield approximately 250 full depth cycles with a capacity $\geq$80% of the theoretical.

3.3.3 Safety of Li/TiS$_2$ vs δ-LiAl/TiS$_2$ Cells

From abuse tests performed with AA-size cells after five cycles an evaluation of the relative safety of secondary TiS$_2$ cells containing Li or LiAl anodes can be made. Figure 9 shows the effect of heating AA cells containing the standard electrolyte. Figure 9a represents data for Li/TiS$_2$ while 9b represents data collected with a 70 LiAl/TiS$_2$ couple. In both instances an exotherm began at approximately 150°C; the maximum temperature was 300°C for the cell with the Li anode and 235°C for the one with the 70 LiAl alloy. For the Li/TiS$_2$ cell, the OCV was constant at 2.38V until it started to drop at ~140°C, falling sharply when the exotherm occurred. The OCV dropped from 2.38V to 0V at 128°C for the cell having the alloy. Both cells exploded by rupture of the weld between the cover and the can.

AA cells were also shorted (after a brief cycling period) while the temperature, OCV, and current were recorded. Figure 10 shows data collected for the shorting of the two cells containing the dioxolane ternary electrolyte. Figure 10a corresponds to the cell with the Li anode, and 10b pertains to data from the cell with the 70 LiAl anode. For the two cells represented by Figure 10 the maximum

16
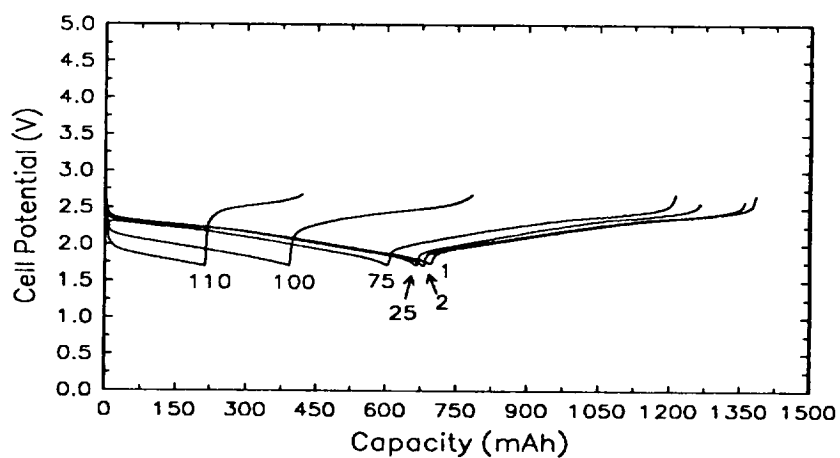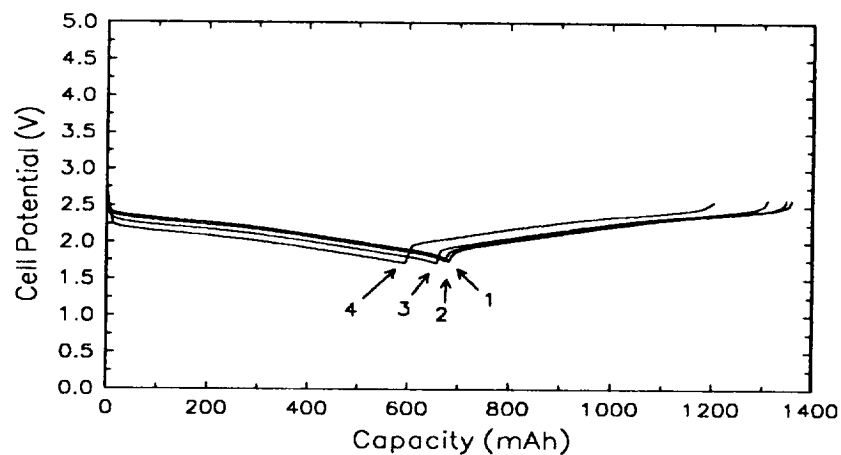
Fig. 7. Cycling curves from (a) capacity/rate and (b) long term cycling studies performed with a AA-size 70 LiAl/TiS$_2$ cell containing the standard binary electrolyte. All cycles in (a) had charge current densities of 0.75 mA/cm^2; discharge current density was 0.75, 1.5, 3, and 5 mA/cm^2, respectively, for cycles 1 through 4. All cycles in (b) were performed at 1.4 mA/cm^2 for discharge and 0.75 mA/cm^2 charge.

17
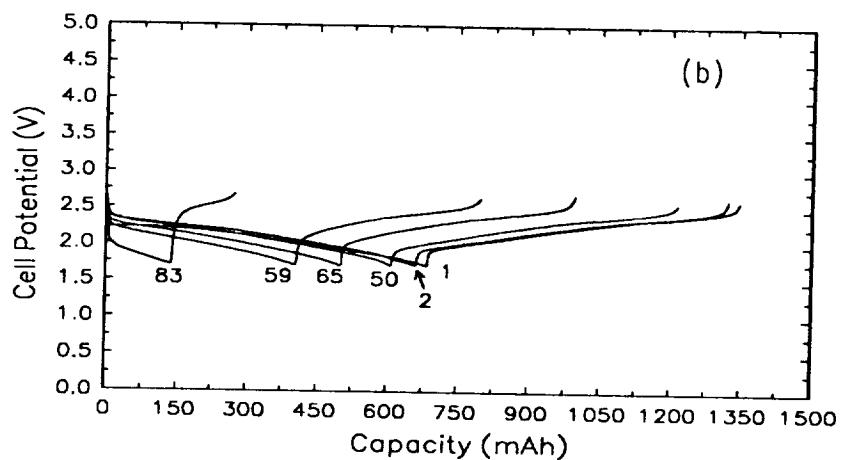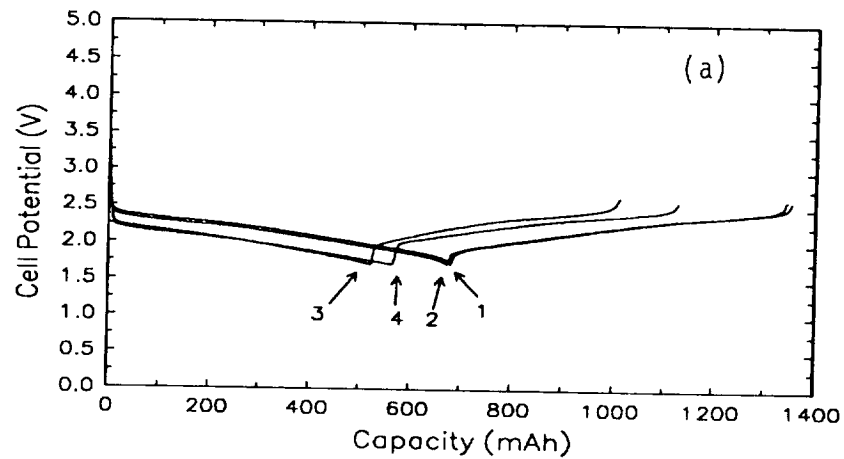
Fig. 8. Cycling curves from (a) capacity/rate and (b) long term cycling studies performed with a AA-size 70 LiAl/TiS$_2$ cell containing the dioxolane ternary electrolyte. All cycles in (a) had charge current densities of 0.75 mA/cm^2; discharge current density was 0.75, 1.5, 3, and 5 mA/cm^2, respectively, for cycles 1 through 4. All cycles in (b) were performed at 1.4 mA/cm^2 for discharge and 0.75 mA/cm^2 for charge.

18
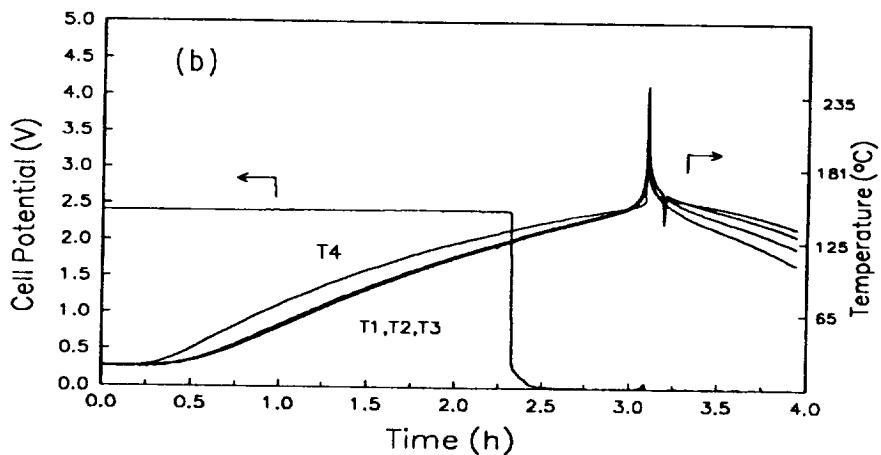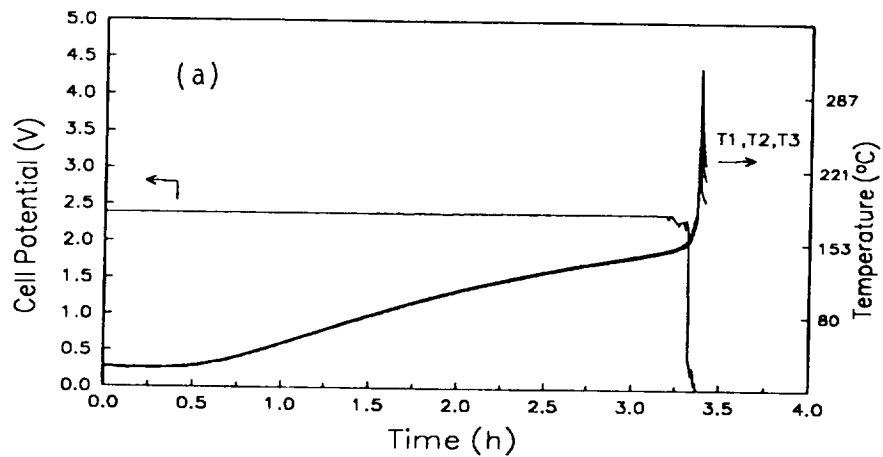
Fig. 9. Results obtained when (a) Li/TiS$_2$ and (b) 70 LiAl/TiS$_2$ AA-size cells containing the standard binary electrolyte were heated after several cycles.
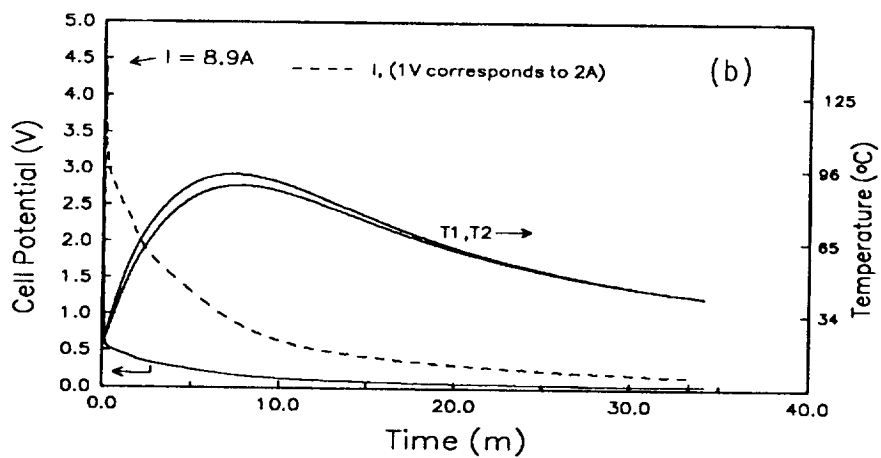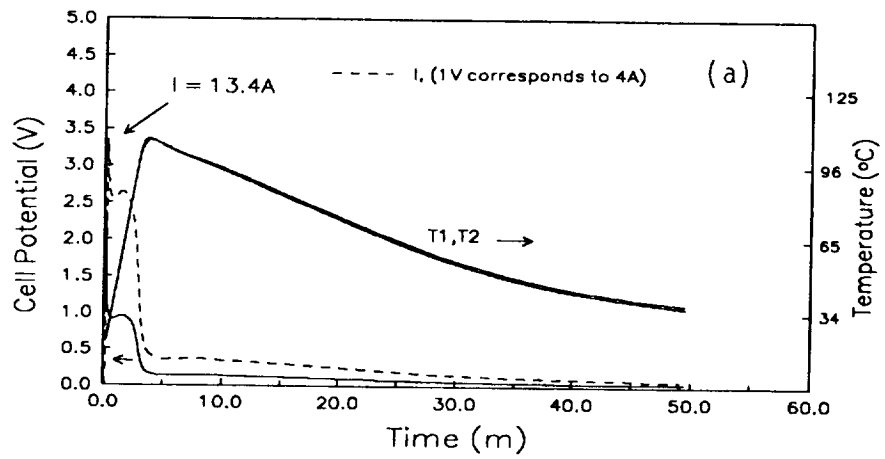
Fig. 10. Results obtained when (a) Li/TiS_2 and (b) 70 $LiAl/TiS_2$ AA-size cells containing the dioxolane ternary electrolyte were shorted after several cycles.

current, 13.5A, was observed with Li and the cell temperature reached 106°C. A current of 8.9A was obtained with 70 LiAl, and the temperature reached 93°C. Neither of these cells ruptured as a result of shorting.

3.4 DSC Studies Pertaining to Safety Related Chemistry of Secondary Li Cells

Use of secondary lithium batteries is restricted severely because of safety concerns and poor cycle life performance (5). These restrictions have been associated with the dendritic lithium deposits which form at the anode as a result of cycling, and the reactivity of inorganic and organic electrolyte components with this high surface area lithium (6-8). Electrolytes commonly used in rechargeable Li cells have included solvents such as THF, 2-MeTHF, PC, EC, dioxolane, or triglyme, and salts such as $LiAsF_6$, $LiClO_4$, and $LiPF_6$. Our preferred electrolyte is a mixture with the composition 48 volume-percent (v/o) THF:48 v/o 2-MeTHF:4 v/o 2-MeF/1.5M $LiAsF_6$ (3).

Differential Scanning Calorimetry was used as a probe to investigate the relationship between the various components and the thermal stability of Li cells. We studied the anodes, solvents, electrolytes, as well as the separator material. We also studied the effect of heat upon solvents and electrolyte solutions in contact with fresh Li foil, and finely divided Li removed from anodes of cycled cells. Cathode materials were also tested before and after cycling. It is to be emphasized that all the samples were prepared in an Argon-filled dry-box and sealed hermetically.

Anodes: The evidence presented above (see Section 3.1) shows clearly that the δ-LiAl alloys are mixtures of elemental lithium and a phase with the stoichiometry Al_4Li_9. Figure 11 shows the DSC data for all the anode materials, including Li, which we have used in the course of this research. The endotherm at 182.8°C corresponds to the melting of lithium, and is reasonably close to the 180.7°C melting point found in the literature. The starting or onset temperature for the melting of the alloys ranges from 183.3°C to 184.3°C, and the multiple peaks indicate the presence of several phase transformations in these materials. From the Al-Li phase diagram we observed that Li melts at 180.7°C, and the Al_4Li_9 phase is involved in an equilibrium at a eutectic temperature of 175±5°C. Equation [3] below shows this equilibrium relationship between the liquid phase, the δ (Al_4Li_9) phase and the body-centered cubic phase of elemental lithium.

$$Liquid \rightleftharpoons Al_4Li_9 + Li_{(s)} \qquad [3]$$
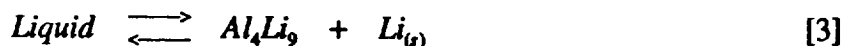
Lithium and LiAsF₆: The DSC scan of a sample consisting of a piece of Li foil and solid $LiAsF_6$ when heated to 245°C showed only the melting of the Li (Fig. 12). An identical sample heated to 290°C shows, in addition to the melting of Li, an exotherm at 245°C and an endotherm at 265°C. These two peaks are approximately equal in size, with peak heights on the order of 0.1 W/g. Above 265°C the reaction is strongly exothermic, with a peak height of nearly 2 W/g.
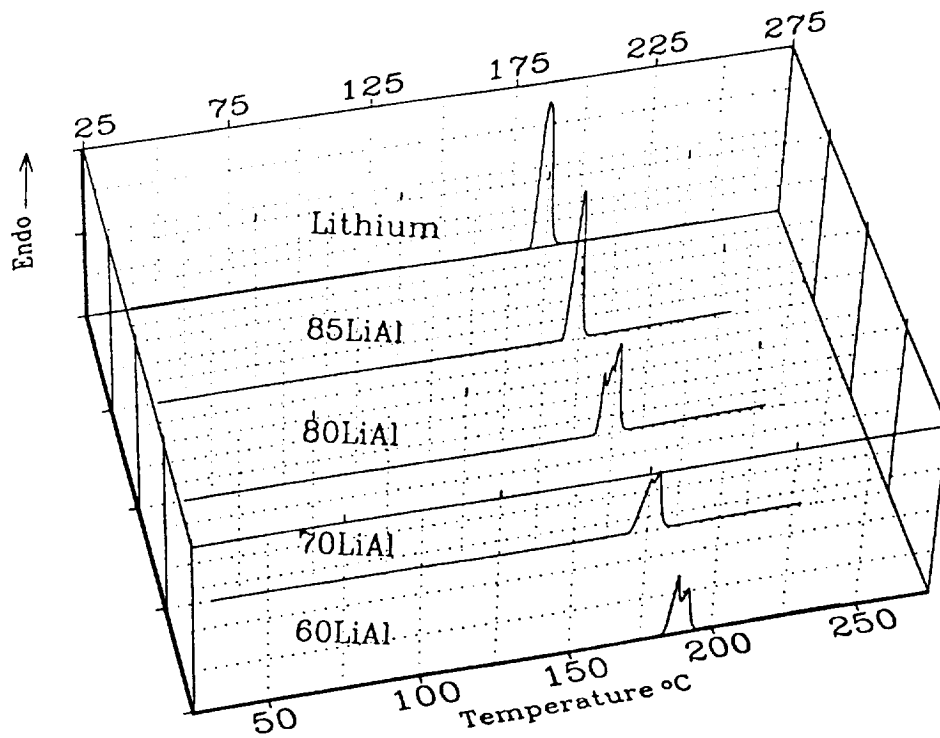
Fig. 11. Comparative DSC data for lithium metal and the alloy anodes.
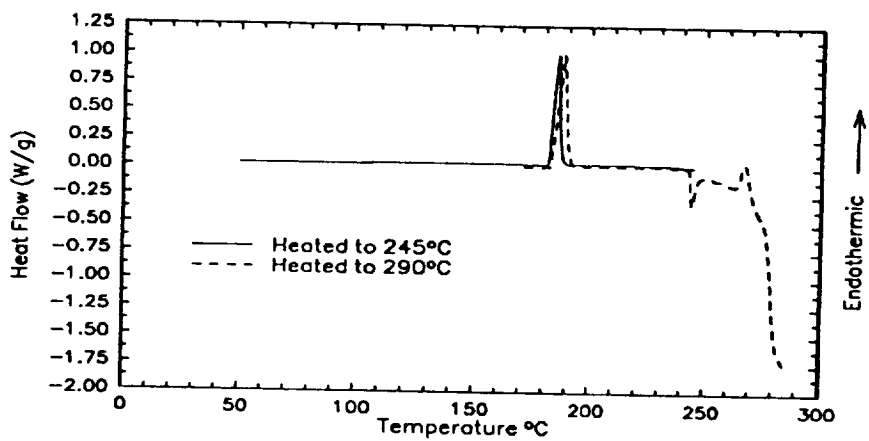
Fig. 12. DSC results obtained with a Li/LiAsF$_6$ mixture.

22

Separator: Celgard was used as the separator in all the cells which we fabricated and tested. In the case of cells having ether-based electrolytes the separator was Celgard 2400; electrolytes containing propylene carbonate were used in cells having Celgard 3401. Celgard is made from isotactic polypropylene, which is reported to melt at 174°C. Celanese states in its literature that "if the film is constrained, it can be used at temperatures up to 127°C for several hours without loss of porosity" (9). Above this temperature, the Celgard becomes less permeable, acting as a more continuous barrier between the anode and cathode. This phenomenon would influence cell performance only if the cell temperature was not allowed to go much above this point, the cell was cooled instantaneously, and cycling continued. For such a case, the decreased separator porosity would only become apparent when electrolyte flow was too restricted to support certain rates. The reported melting point for the 2000 Series materials is 168°C. The DSC data we obtained for the separator material are shown in Figure 13, and both Celgard 2400 and 3401 start melting at 160-161°C. The phase transformation appears complete at 164-165°C. The figure also shows the results for repetitive tests with the same sample (Celgard 2400, runs 1 and 2) in which the sample was heated to 290°C each time. The endotherm associated with melting is broader the second time around, but the melting range of the polymer is not much changed.

Solvents: Figure 14 is a composite which shows that the result of heating the solvent mixture 48 volume-percent (v/o) THF:48 v/o 2-MeTHF:4 v/o 2-MeF, or the pure solvents, EC and PC. No exothermic reactions occur even when these samples are heated to 290°C. Similar observations were made for similar experiments performed using pure dioxolane or triglyme. Only the experiment with ethylene carbonate shows an endothermic peak, and it is attributed to the melting of this solid at 40°C.

Solvents on Li foil: The highly reactive nature of elemental Li is well known. The ability to use lithium as an anode in cells containing non-aqueous electrolytes is attributable to the formation of passivation layers at the lithium surface which kinetically stabilize the lithium to continued reaction with the electrolyte components. Consequently, it is important to determine the point at which the application of heat supplies enough thermal energy to overcome this kinetic barrier, and also to determine the heat flow for the system. Figure 15 shows the DSC results for a sample which consisted of a piece of Li foil and the THF/2-MeTHF/2-MeF solvent mixture used in our standard binary electrolyte. It shows primarily the melting of Li at 180°C, with a small (<0.1 W/g) exothermic peak at ~125°C.

Alteration of this solvent combination by the addition of dioxolane is not expected to have much of an effect since a Li/dioxolane sample (see Fig. 16) shows a net exotherm of 0.25 W/g in which the heat evolution is very gradual starting at about 100°C, and the characteristic endotherm for the melting of lithium is seen at 180°C.
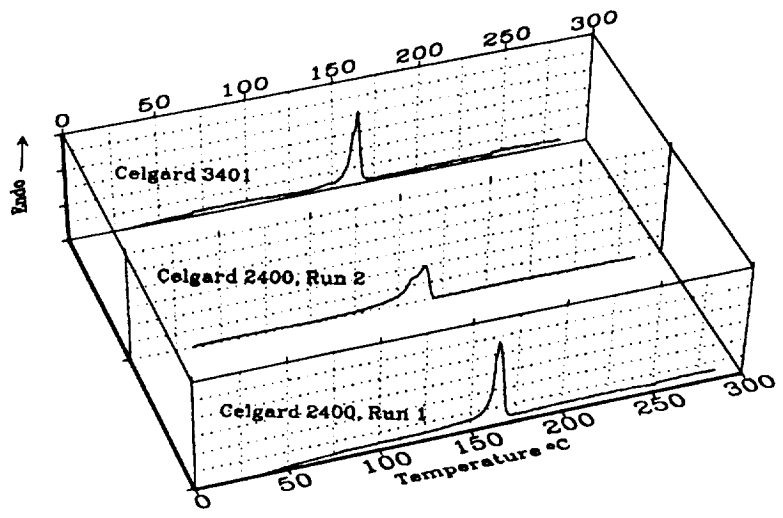
Fig. 13. DSC data for Celgard 2400 and Celgard 3401.
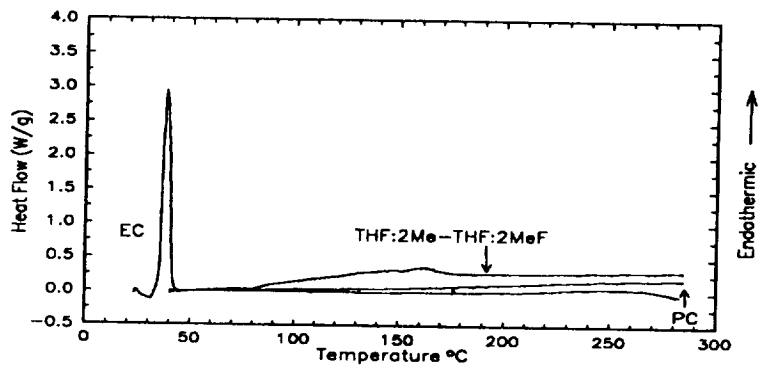
Fig. 14. DSC results for ethylene carbonate, propylene carbonate, and the 48 v/o THF:48 v/o 2-MeTHF:4 v/o 2-MeF solvent mixture.
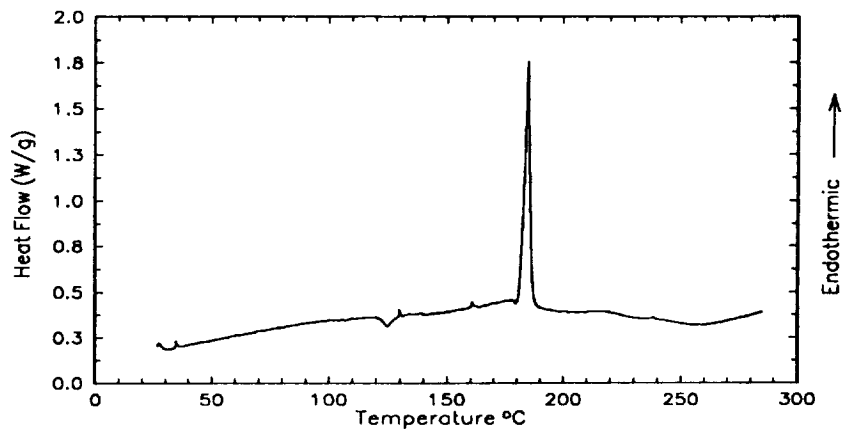
Fig. 15. DSC results for fresh lithium foil wet with a solvent mixture with the composition 48 v/o THF:48 v/o 2-MeTHF:4 v/o 2-MeF.
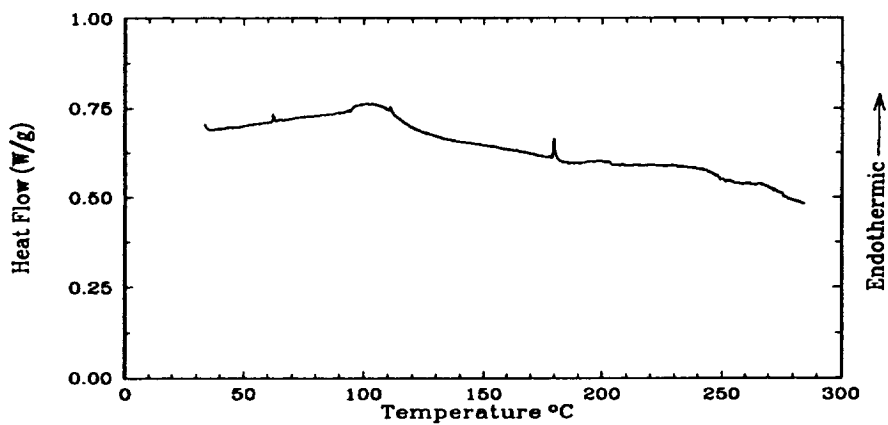
Fig. 16. DSC results for a fresh lithium foil wet with pure dioxolane.

Of the other solvents, Li/PC (Fig. 17) and Li/EC (Fig. 18) show primarily the melting of the Li foil. Li/Triglyme (Fig. 19), however, undergoes an exothermic reaction starting at about 110°C. The net exotherm is approximately 0.25 W/g by the time the Li melts, at which point a broad, multi-peak band with a maximum of 3.5 W/g is observed. The maximum occurs at 190°C, and the baseline is recovered at approximately 210°C.

*Electrolytes*: Figure 20 shows DSC data obtained for a fresh (unused) aliquot of the 48 (v/o) THF:48 v/o 2-MeTHF:4 v/o 2-MeF/1.5M LiAsF$_6$ electrolyte. The exothermic reactions are evident between about 140°C and 200°C. It is important to note several points. **First**, *the exotherms observed in this experiment occur in the absence of elemental lithium. Second, the evolved heat is maximized at about the temperature which corresponds to the melting point of Celgard.* This result suggests that the particular electrolyte selected may be an important contributory factor to the instability of a secondary Li cell exposed to an elevated temperature. Heat released by reactions involving the electrolyte may be sufficient to raise the internal cell temperature to the point that the separator may melt although the external temperature is maintained below the melting point. Of course, once the separator is violated, a direct short is possible between the anode and the cathode, and catastrophic failure may be expected.

The ternary electrolyte with the composition 48 v/o THF:28 v/o Dioxolane:20 v/o THF:4 v/o 2-MeF/LiAsF$_6$ (1.5M) was also found to undergo strong exothermic reactions which began at about 150°C. Figure 21 shows the largest peak to have an intensity of 2.7 W/g at 160°C. The exotherm appears in two regions, the first from 148 to 177°C and the second from about 177°C to 194°C. A comparison of these results those for the THF:2-MeTHF binary indicate that the addition of dioxolane does not improve the thermal stability of the electrolyte, and that a significant exothermic reaction occurs well below the melting point of lithium.

In order to determine which electrolyte components are the strongest contributors to the exotherms observed in the experiments described above for the standard electrolyte and the one containing dioxolane, samples of THF/LiAsF$_6$ (1.5M), 2-MeTHF/LiAsF$_6$ (1.5M), and 2-MeF/LiAsF$_6$ (saturated) were analyzed. Figures 22 through 24 show the results obtained. Clearly, both THF and 2-MeTHF are involved in very strong exothermic reaction with LiAsF$_6$. In the case of THF, significant reaction starts at 178°C. It is characterized by an initial endothermic spike equivalent to approximately 0.25 W/g followed by exothermic maxima at 180°C, 200°C, and 213°C. Comparison of these figures show the maxima to be more clearly resolved in the case of THF than those observed with 2-MeTHF (170°C, 173°C, and 178°C). Other samples of THF/LiAsF$_6$ (1.5M) showed a broad continuous exotherm very much like the one in Figure 23. In any event the data show clearly that there is clearly an exothermic reaction between LiAsF$_6$ and both THF and 2-MeTHF. In the standard electrolyte, 2-MeF is used as an additive which we have found to improve dramatically the cycle life of cells with electrolytes having THF as a principal component. LiAsF$_6$ is only sparingly soluble in 2-MeF, and the DSC data shown in Figure 24 were collected from a sample of 2-MeF which was saturated with LiAsF$_6$ at room temperature. The data show no evidence of strong endothermic or exothermic reactions.
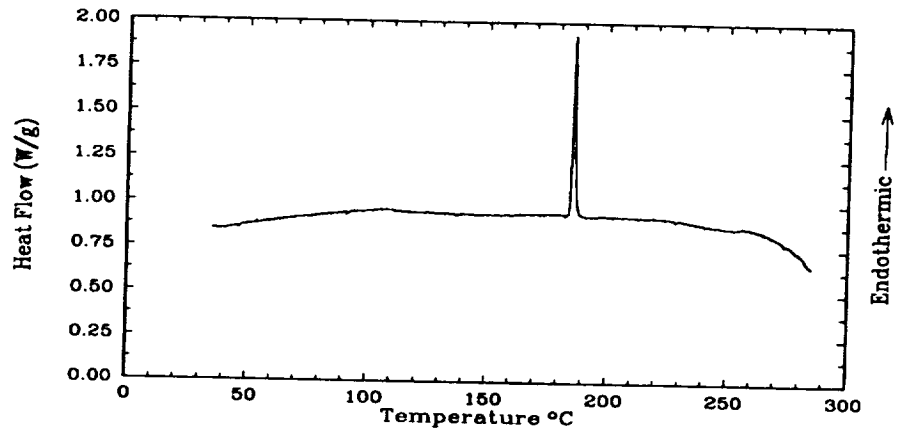
Fig. 17. DSC results for fresh lithium foil wet with pure propylene carbonate.
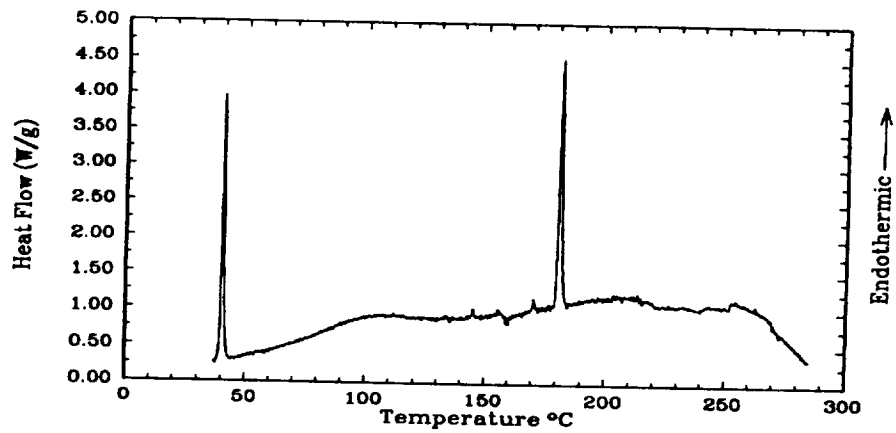
Fig. 18. DSC results for fresh lithium foil mixed with ground ethylene carbonate.
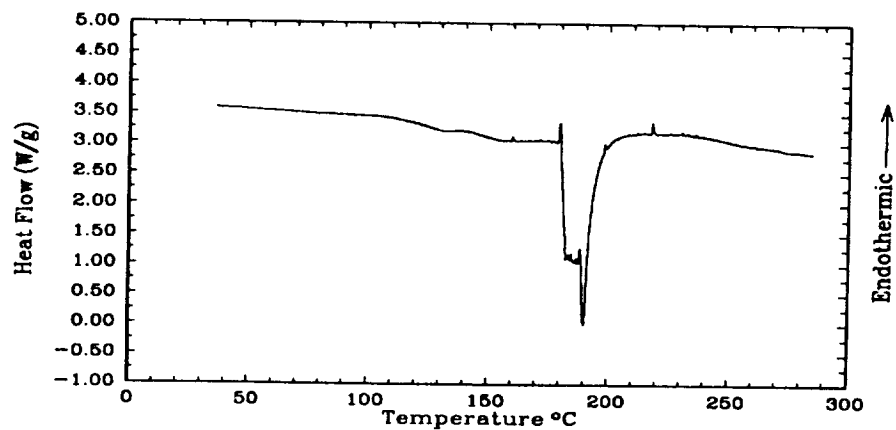
Fig. 19. DSC results for fresh lithium foil mixed with pure triglyme.
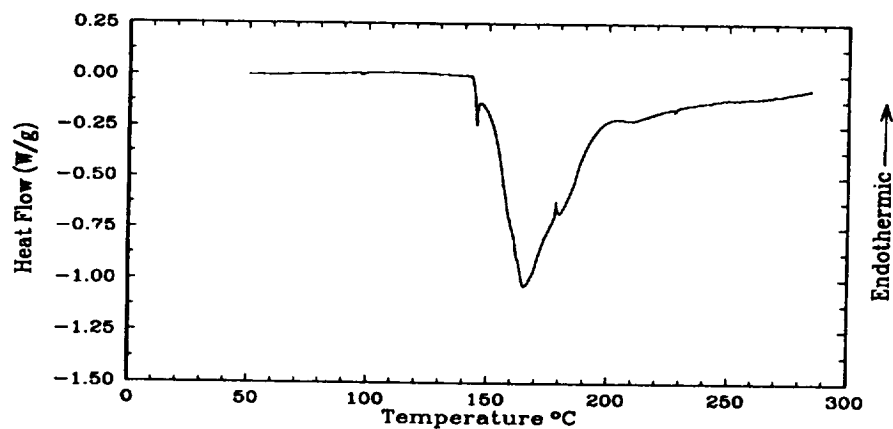
Fig. 20. DSC results for unused 48 v/o THF:48 v/o 2-MeTHF:4 v/o
2-MeF/LiAsF$_6$ (1.5M) electrolyte.
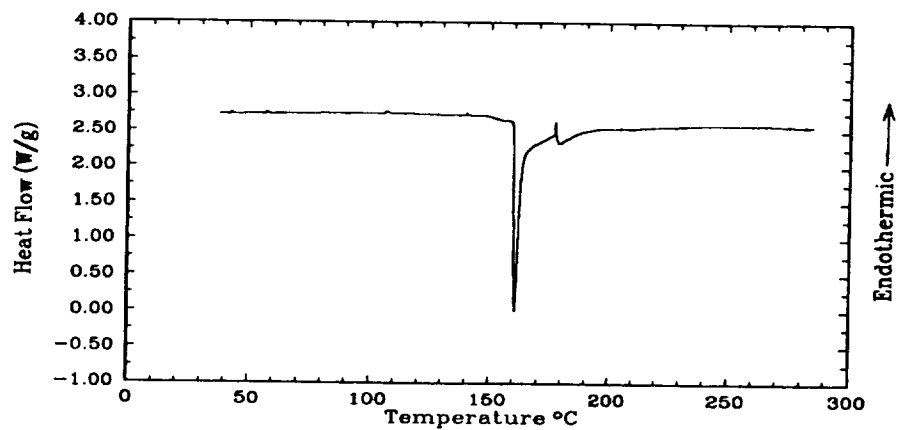
Fig. 21. DSC results for unused 48 v/o 2-MeTHF:28 v/o Diox:20 v/o THF:4 v/o 2-MeF/1.5M LiAsF$_6$ electrolyte.
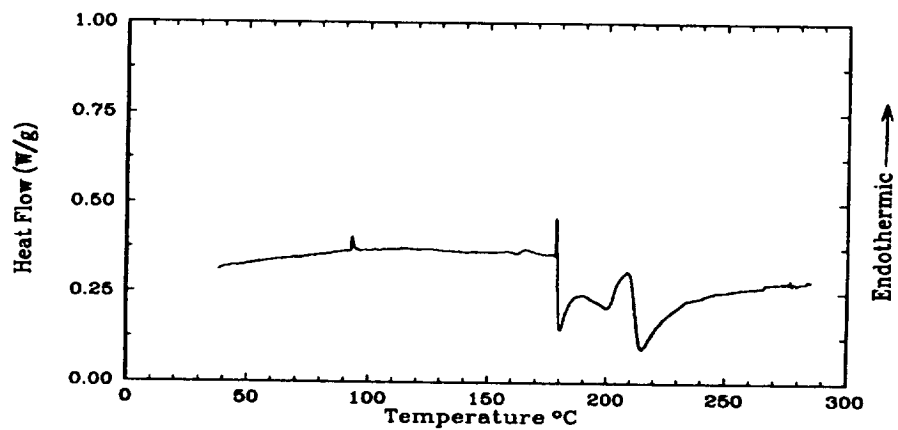
Fig. 22. DSC results for THF/LiAsF$_6$ (1.5M).

29
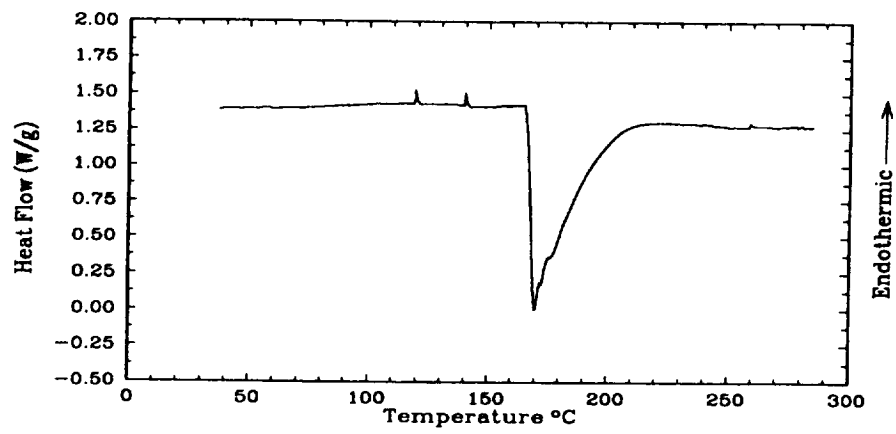
Fig. 23 DSC results for 2-MeTHF/LiAsF$_6$ (1.5M).
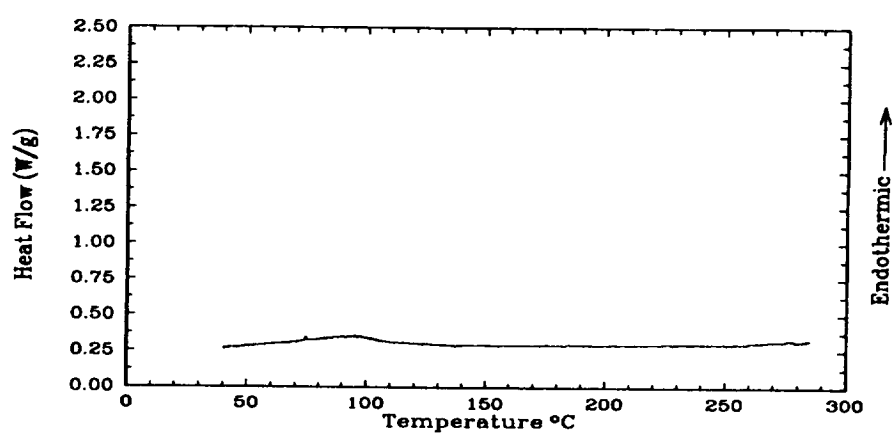
Fig. 24. DSC results for 2-MeF/LiAsF$_6$ (saturated).

30

After normalization for the sample mass, it appears that the reaction between 2-MeTHF and LiAsF$_6$ contributes most of the heat to the exothermic reaction which we first observed for the unused standard electrolyte. **IT IS PARTICULARLY IMPORTANT TO NOTE THAT THIS EXO-THERMIC BEHAVIOR IS IN THE COMPLETE ABSENCE OF LITHIUM, EITHER AS FOIL OR AS THE FINELY DIVIDED ANODE RESIDUE WHICH CAN BE REMOVED FROM CYCLED CELLS, AND THAT IT COVERS A BROAD TEMPERATURE RANGE WHICH STARTS WELL BELOW THE LITHIUM MELTING POINT.**

Electrolytes containing propylene carbonate or propylene carbonate blended with ethylene carbonate can cycle lithium efficiently. The tendency of these solvents to form a passivation layer at the anode surface which limits the reactivity of the lithium with the solvent is appealing when shelf-life is considered. These solvents are inherently safer to work with than ethers, and consequently it was important to use Differential Scanning Calorimetry to assess the thermal properties of electrolytes containing them. The basic electrolyte is one containing equal volumes of PC and EC with a LiAsF$_6$ concentration of 1.0M. Figure 25 shows the effect of heating an aliquot of this electrolyte. The endotherm at ~190°C corresponds to the boiling point of 1,2-propanediol, a common impurity in propylene carbonate. Vaporization of this contaminant seems to coincide with the exotherm which occurs at 195°C in the presence of LiAsF$_6$. A similar experiment performed with PC/LiAsF$_6$ (1.0M) (Fig. 26) supports this concept, showing that the source of the endotherm and subsequent exotherm is the propylene carbonate, and does not appear to involve the ethylene carbonate.

Dioxolane, used as a component of the ternary electrolyte containing THF and 2-MeTHF, undergoes a very strongly exothermic reaction at 158°C (see Fig. 27). A gradual exotherm begins at 145°C, followed by a small (~0.25 W/g) endotherm at 158°C. An almost immediate 4 W/g exotherm follows at 160°C. This exotherm appears to have a second peak at 169°C, and the exotherm ends by the time the temperature reaches 187°C.

Figure 28 shows that the triglyme/LiAsF$_6$ (1.0M) solution generates a significant exotherm at 250°C (3.5 W/g). This is apparently of little consequence when triglyme is present as approximately one-third of the solvent in the ternary electrolyte with the composition 35 v/o PC:35 v/o EC:30 v/o triglyme/LiAsF$_6$ (1.0M) (Fig. 29).

Electrolytes on Li foil: Figures 30 through 32 show the results obtained when Li foil was heated in the presence of the THF:2-MeTHF:2-MeF/LiAsF$_6$, THF:2-MeTHF:Dioxolane:2-MeF/LiAsF$_6$ or PC:EC:Triglyme/LiAsF$_6$ respectively. The data for the ether containing electrolytes are characterized by strong exotherms which correspond to those described above for the electrolytes alone, and an endothermic peak at approximately 180°C which corresponds to the melting of lithium. In each case (Figs. 30,31), the predominant exotherm occurs at temperatures below the melting point of lithium. These data and those obtained with the electrolytes alone seem to show that the melting of lithium is not a prerequisite for the evolution of heat in a cell containing lithium. Figure 32 shows
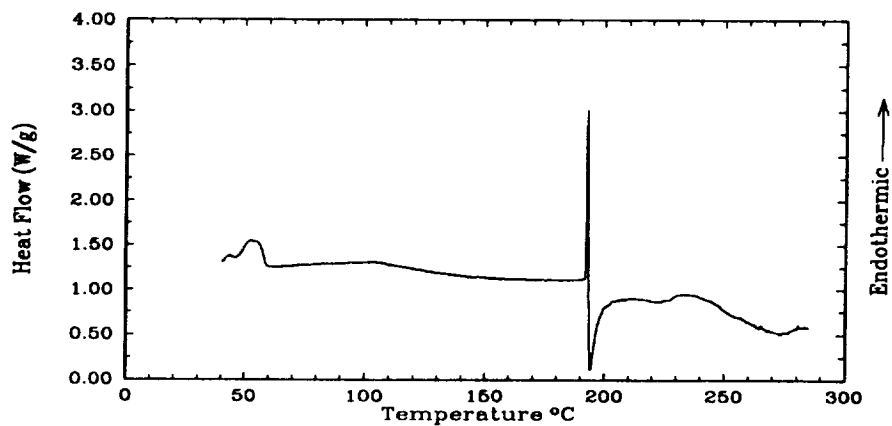
Fig. 25. DSC results for 50 v/o EC:50 v/o PC/LiAsF$_6$ (1.0M).
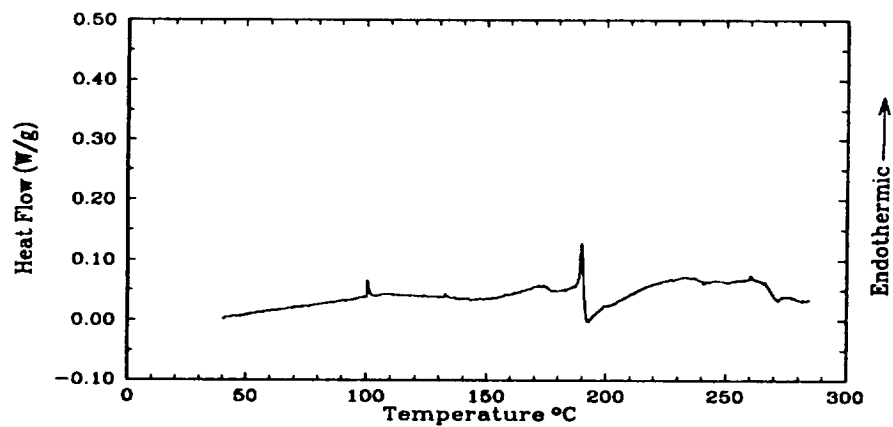
Fig. 26. DSC results for PC/LiAsF$_6$ (1.0M).

32
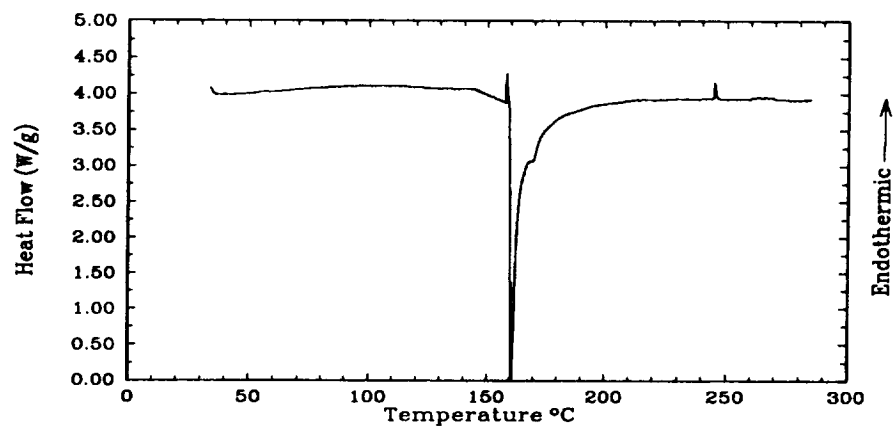
Fig. 27. DSC results for Dioxolane/LiAsF$_6$ (1.5M).
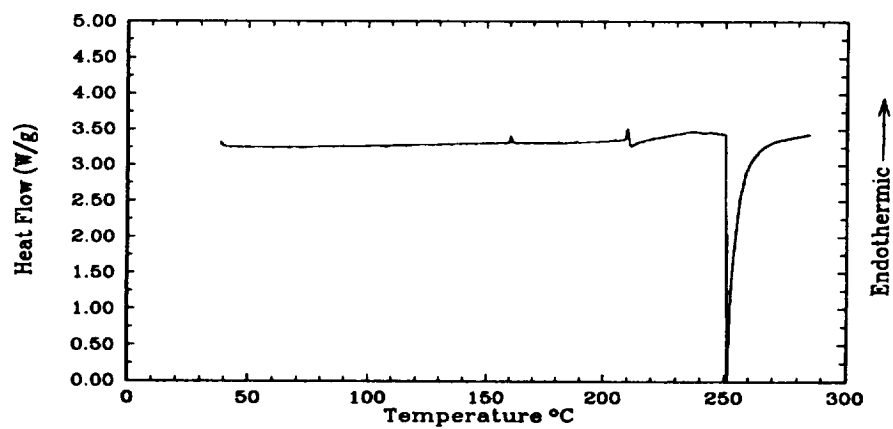
Fig. 28. DSC results for triglyme/LiAsF$_6$ (1.0M).

33
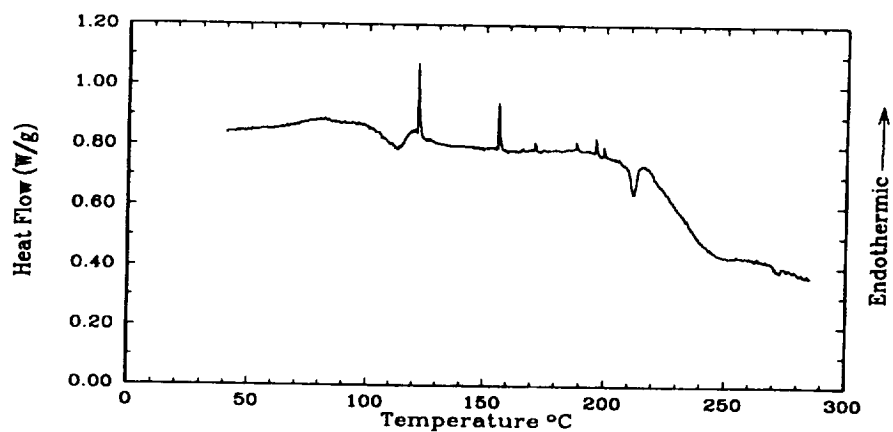
Fig. 29. DSC results for the 35 v/o PC:35 v/o EC:30 v/o triglyme/LiAsF$_6$ (1.0M) electrolyte.
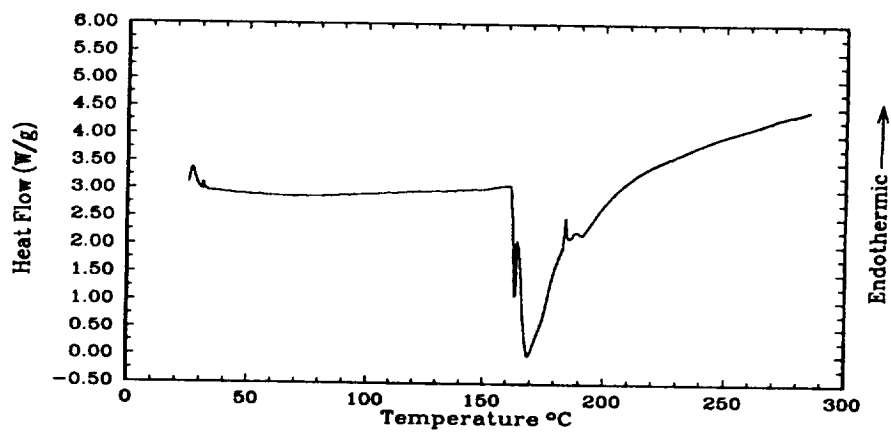
Fig. 30. DSC results for the reaction between Li foil and 48 v/o THF:48 v/o 2-MeTHF:4 v/o 2-MeF/LiAsF$_6$ (1.5M) electrolyte.

34

that the predominant reaction in the case of the Li/PC:EC:Triglyme (LiAsF$_6$) sample is the melting of lithium at 180°C. There is some apparent exothermic contribution (probably due to the triglyme/LiAsF$_6$ reaction described above) but it occurs at temperatures above 210°C, and reaches a maximum of only 0.5 W/g at the final (290°C) temperature.

High surface area Li removed from cycled anodes: After cycling, the anodes in secondary Li cells are coated with a granular, brown deposit. This material is mostly high surface area Li which is not in good electronic contact with the anode current collector. The color is attributable to the reaction products of the electrolyte reduced on the lithium surface. Samples of the wet, granular deposits are easily removed form disassembled cells for analysis, and Figures 33 and 34 are DSC data obtained for such materials removed from the anode of cycled 85 LiAl/TiS$_2$ cells containing electrolytes with the composition 48 v/o THF:48 v/o 2-MeTHF:4 v/o 2-MeF/LiAsF$_6$ (1.5M) and 48 v/o 2-MeTHF:28 v/o Diox:20 v/o THF:4 v/o 2-MeF/1.5M LiAsF$_6$, respectively. In both cases exotherms extend over a broad temperature range starting at approximately 100°C. The DSC data for the THF:2-MeTHF:2-MeF/LiAsF$_6$ electrolyte has a single peak with a width of approximately 70°C, while the electrolyte containing dioxolane shows multiple peaks and spreads from about 100°C to 200°C. Reaction products removed from the anodes of similar cells containing 35 v/o PC:35 v/o EC:30 v/o Triglyme/1.0M LiAsF$_6$ (Fig. 35) or 50 v/o PC:50 v/o EC:1.0M LiAsF$_6$ (Fig. 36) show exothermic activity starting at 50°C. These results agree with recent Accelerating Rate Calorimetric studies (10) of the reaction between high surface area lithium and 50 v/o EC:50 v/o PC/1M LiAsF$_6$ which show three separate exothermic events between 120°C and 215°C.

Cycled cathode materials: Unlike the anode, it is expected that a cathode removed from a fully charged cell will be free of elemental lithium. Thermal studies performed with material removed from such a cathode can be expected to yield results which reflect reactivity in the absence of lithium. Accordingly, after extensive full-depth cycling, cathode material was removed from a cell having the 48 v/o 2-MeTHF:28 v/o Dioxolane:20 v/o THF:4 v/o 2-MeF/1.5M LiAsF$_6$ electrolyte after the cell was fully charged. The DSC data for this material are graphed in Figure 37, and the curve has a shape similar to the one for the material removed from the anode of a cycled cell having the same electrolyte (see Fig. 34). In both instances, exothermic reaction occurs. (In the case of the material removed from the anode, the presence of elemental lithium is indicated by the endotherm at 180°C, the lithium melting point). The initial exotherm starts at approximately 100°C for both the material obtained from the anode and the one removed from the cathode. Although the data are normalized for the sample mass, the maxima and the breadth of the exotherm in the case of the material from the anode are much greater. This phenomenon may reflect the presence of a significant number of lithium fines in this sample compared to virtually none in the cathode material. While the presence of Li fines can surely enhance the exothermic behavior, it is not necessary, and TiS$_2$ may catalyze the electrolyte decomposition.

36
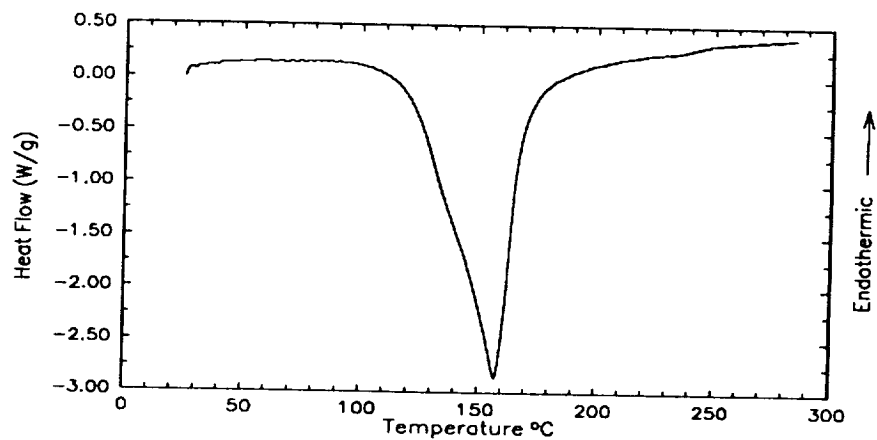
Fig. 33.   DSC data for the reaction product removed from the anode in an 85 LiAl//48 v/o THF:48 v/o 2-MeTHF:4 v/o 2-MeF/1.5M LiAsF$_6$//TiS$_2$ cell.
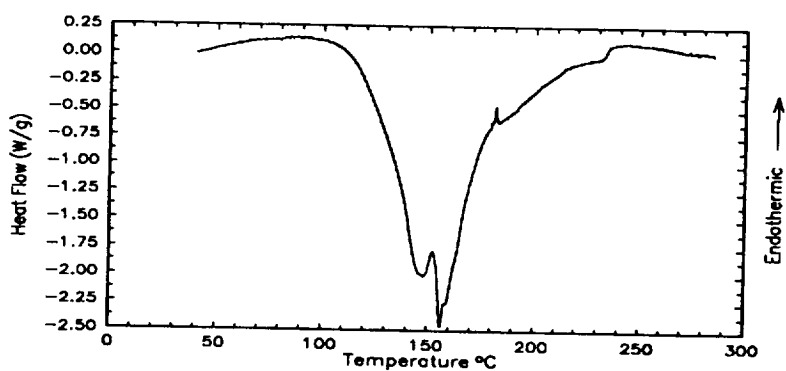
Fig. 34.   DSC data for the reaction product removed from the anode in an 85 LiAl//48 v/o 2-MeTHF:28 v/o Dioxolane:20 v/o THF:4 v/o 2-MeF/1.5M LiAsF$_6$//TiS$_2$ cell.

37
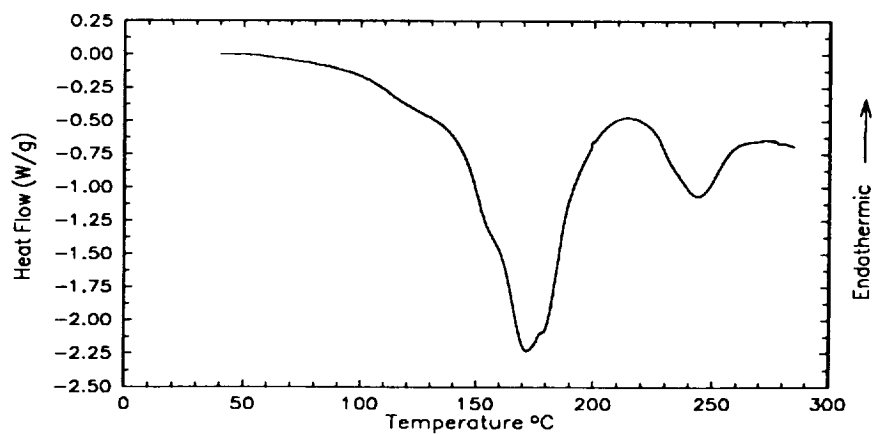
Fig. 35. DSC data for the reaction product removed from the anode in an 85 LiAl//35 v/o PC:35 v/o EC:30 v/o Triglyme/1.0M LiAsF$_6$//TiS$_2$ cell.
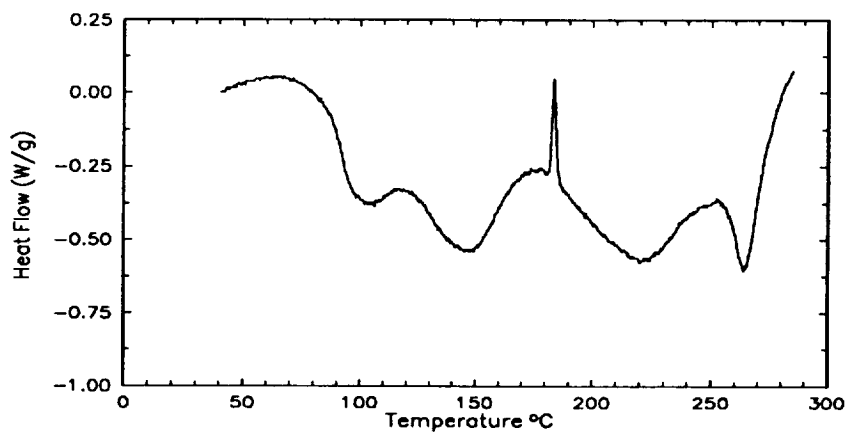
Fig. 36. DSC data for the reaction product removed from the anode in an 85 LiAl//50 v/o PC:50 v/o EC/1.0M LiAsF$_6$//TiS$_2$ cell.
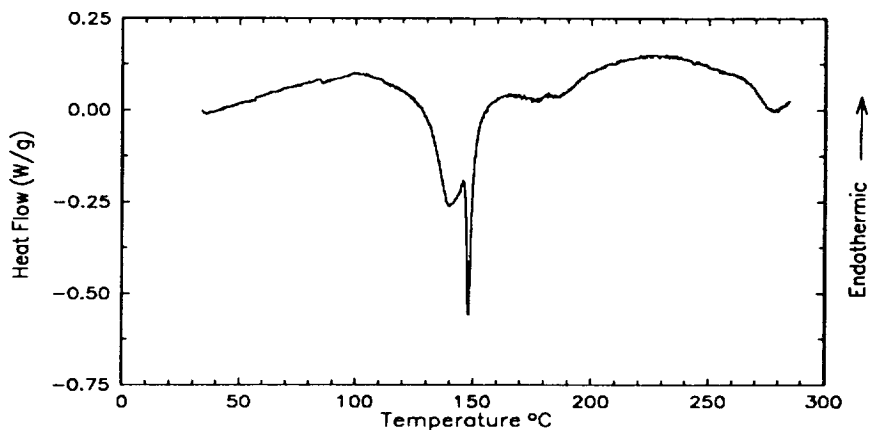
Fig. 37.   DSC data for material removed from a TiS₂ cathode after full depth cycling in the 48 v/o 2-MeTHF:28 v/o Dioxolane:20 v/o THF:4 v/o 2-MeF/1.5M LiAsF₆ electrolyte. Cycling was terminated with the cathode fully charged.

3.5   Carbon Anodes

The same thermodynamic properties which make lithium attractive as a low density energy source are also responsible for deterioration of electrolyte and the propensity for catastrophic cell failure. The δ-LiAl alloys were seen as one possible alternative to pure Li foil anodes. Use of such a material would provide immediate safety advantages by significantly limiting the amount of elemental lithium in the cell while maintaining much of the energy to be derived from the use of an electro-chemical cell which depends upon the movement of Li ions.

Carbon has received much recent attention as the basis for an alternate Li ion electrode in which a Li intercalated carbon would contain a reservoir of Li ions without an excess of elemental lithium. Carbons available for use as anode materials include graphite and petroleum coke. While graphite has a crystalline, well-ordered structure, the petroleum cokes differ principally by having only short-range order, without the extensive parallel planes found in graphite. We have performed some preliminary studies involving the use of both petroleum cokes and graphite as the anode material. These studies have involved both the Li$_x$C/TiS$_2$ and Li/C couples.

39

3.5.1 Petroleum Coke

Li_xC/TiS_2 Cells: Figure 38 shows X-ray diffraction patterns obtained with (a) graphite and (b) petroleum coke. The graphite samples have diffraction lines with the d-space values, relative intensities and (hkl) assignments shown in Table 5. Petroleum coke samples showed only a weak, broad, diffraction line centered at approximately 3.5 Å.

(a)

(b)
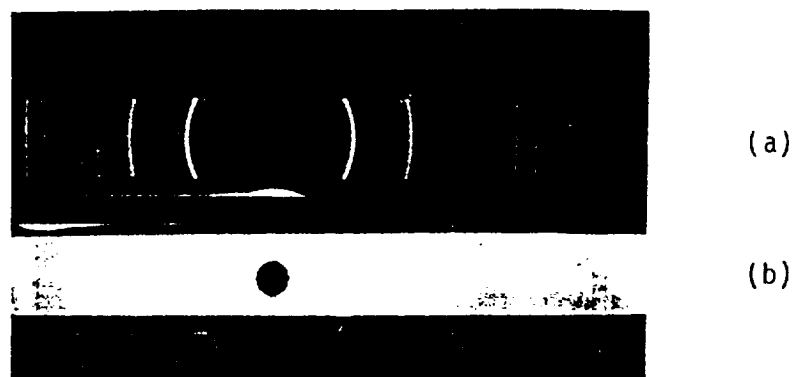
Fig. 38. Debye-Scherrer X-ray diffraction patterns of (a) graphite, and (b) petroleum coke.

Table 5. X-ray Diffraction Data of Graphite Samples

d (Å)	I/I$_o$	hkl
3.28-3.42	100	002
2.10-2.14	8	100
2.00-2.04	20	101
1.67-1.69	10	004
1.225-1.237	15	110
1.151-1.160	10	112

Li$_x$C/TiS$_2$ Cells: Electrodes were fabricated using Asbury 4491, Unocal, or Conoco petroleum coke, and cells were constructed in which one of these carbon electrodes was sandwiched between a Li foil and a TiS$_2$ electrode. Initial cycling was conducted between the carbon and the lithium in order to charge the carbon with the maximum amount of lithium. After several cycles of the Li/C couple, leads were switched to allow cycling between the Li$_x$C and TiS$_2$. Tables 6 and 7 show the discharge/charge capacity, expressed as Li/C$_6$, obtained with Asbury 4491 and Unocal petroleum coke, respectively. The cathodes in these cells were prepared by the pasting method. For clarity, the capacity is expressed as a Li/C$_6$ mole ratio, whether cycling is between Li and C or Li$_x$C$_6$ and TiS$_2$. Both Asbury 4491 and Unocal petroleum coke show initial capacities of ~0.4 Li/C$_6$, but the capacity decays with continued cycling. Figures 39 and 40 show typical cycling curves obtained with these two carbons. In each case the first part of the figure shows the Li/C couple, while the second portion shows the curves for the Li$_x$C$_6$/TiS$_2$ couple. Both carbons show initial specific capacities of ~0.4Li/C$_6$, and within 10 cycles this capacity is reduced approximately by half. When the leads are arranged to cycle lithium between Li$_x$C$_6$ and TiS$_2$, the capacity starts at just less than 0.2 Li/C$_6$. After 57 cycles, the capacity is 0.08 Li/C$_6$ for the Asbury petroleum coke; the Unocal material has a capacity of 0.05 Li/C$_6$ after 54 cycles.

Electrode Stack Pressure: Table 8 shows the results obtained when a Li/C cell containing a 0.015 cm (~6 mil) electrode prepared using the Conoco 5-6 μm petroleum coke and the dipping procedure was cycled. It appears that one of the limitations to the performance of the petroleum coke electrodes made by the pasting procedure was the lack of uniformity of the electrode thickness. Use of the dipping method allows more facile preparation of thin, uniform electrodes. We have fabricated and tested two cells having identical electrodes prepared by this process and containing the same carbon. In one case, the cell had our regular configuration with stack pressure applied by shims placed between the Teflon hemicylinders and the can wall. In the second case, a cell (Fig. 41) was used and a specific (200 psi) constant stack pressure was applied. The performance of these two

41

Table 6.   Capacity vs. Cycle Number for A Cell containing Asbury 4491 Petroleum Coke.

Couple	Cycle	Capacity	
		Li/C_6 (Discharge)	Li/C_6 (Charge)
Li vs. C	1	0.42	0.35
	2	0.38	0.35
	3	0.26	0.26
	4	0.24	0.24
	5	0.23	0.22
	6	0.19	0.18
	7	0.20	0.20
	8	0.17	0.06
	9	0.23	---
Li_xC_6 vs. TiS_2	10	0.19	0.15
	11	0.14	0.13
	20	0.13	0.13
	30	0.11	0.11
	40	0.09	0.09
	50	0.09	0.09
	57	0.08	0.08

Table 7.   Capacity vs. Cycle Number for A Cell containing Unocal Milled Petroleum Coke.

Couple	Cycle	Capacity	
		Li/C_6 (Discharge)	Li/C_6 (Charge)
Li vs. C	1	0.42	0.31
	2	0.30	0.28
	3	0.28	0.27
	4	0.27	---
	5	0.27	0.24
	6	0.26	0.24
	7	0.23	0.23
	8	0.23	0.24
	9	---	0.24
	10	0.24	0.24
	11	0.24	0.24
	12	0.25	0.16
Li_xC_6 vs. TiS_2	13	0.16	0.14
	25	0.12	0.12
	30	0.12	0.11
	40	0.08	0.08
	50	0.07	0.06
	54	0.05	0.05

42
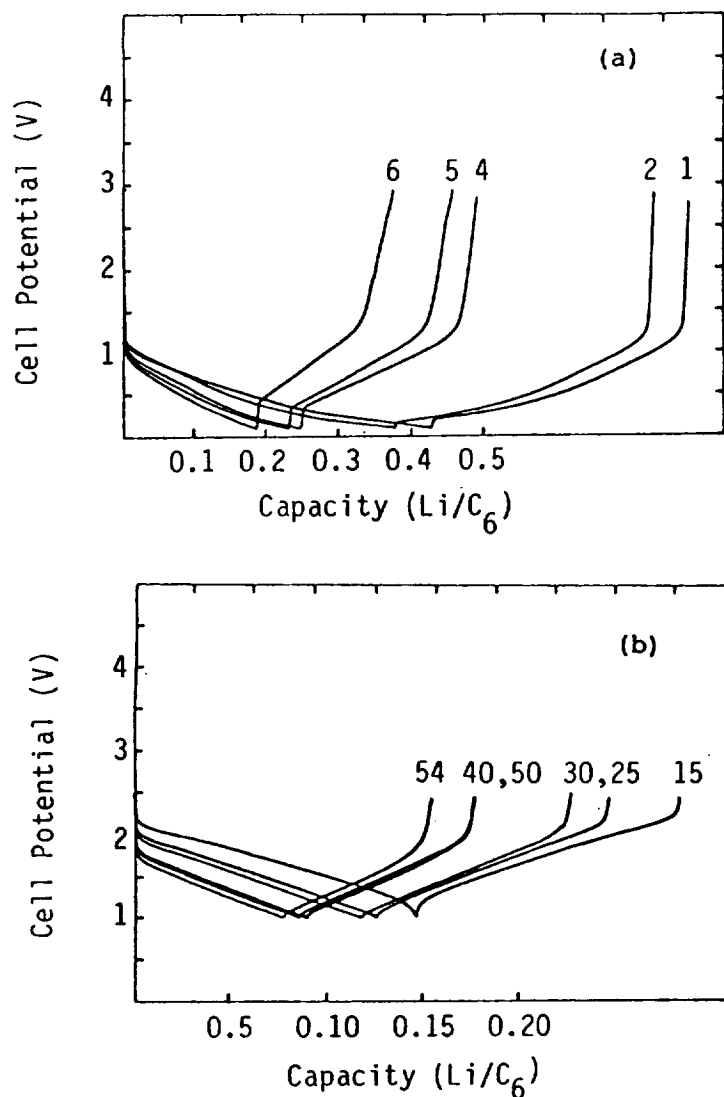
Fig. 39. Cycling curves for (a) Li/C and (b) Li_xC_6/TiS_2 couples in which the carbon electrode was prepared from Asbury 4491 petroleum coke. The carbon electrode measured 2.54 cm x 3.81 cm x 0.046 cm, the electrolyte was PC/1.0M $LiClO_4$, and the current was ±5 mA (±0.1 mA/cm²) for cycles 4-6, and ±1 mA (±0.1 mA/cm²).
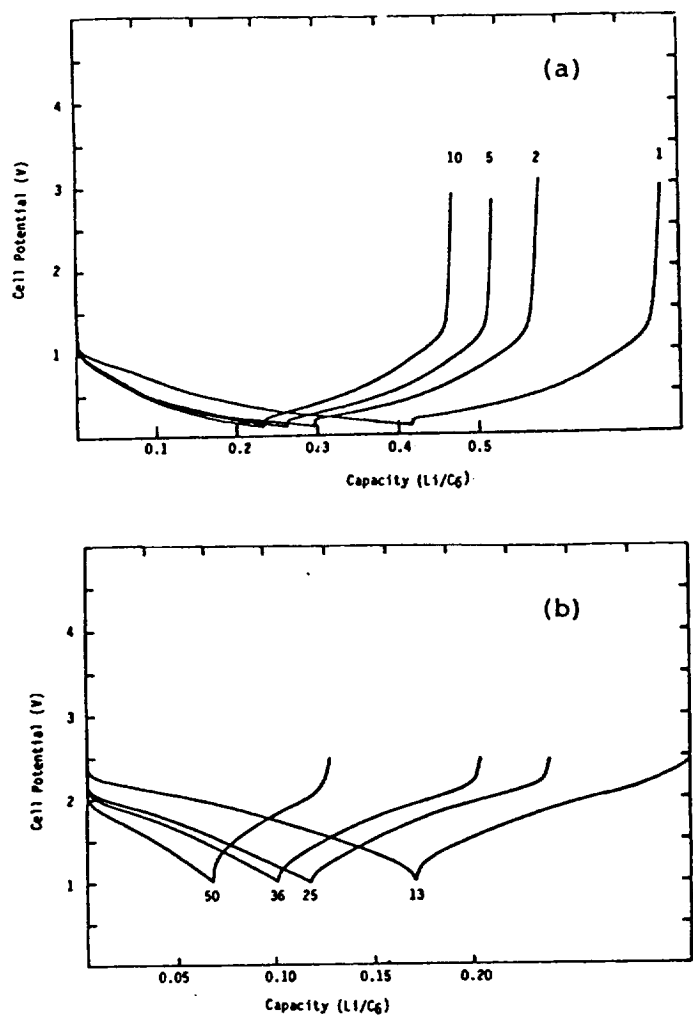
Fig. 40. Cycling curves for (a) Li/C and (b) Li_xC_6/TiS_2 couples in which the carbon electrode was prepared from Unocal petroleum coke. The carbon electrode measured 2.54 cm x 3.81 cm x 0.046 cm, the electrolyte was PC/1.0M $LiClO_4$, and the current was ±1 mA (±0.1 mA/cm^2).

Table 8. Capacity vs. Cycle Number for Conoco, 5-6 μm.

Cycle	Standard Cell Configuration	200 psi Stack Pressure
	Li/C_6	Li/C_6
1	0.48	0.42
2	0.36	0.32
10	0.33	0.29
20	0.32	0.31
24	0.32	0.30*
30*	0.31	---

*Rate studies began after this cycle.

TOP VIEW

CATHODE

NI TAB SANDWICH

1.125

2 cm   COATED AREA = 5 cm2

2.5 cm

1.255 ID

SOFT-SEAL "D" CAN

BELLEVILLE WASHERS (4)

#8-32 NUTS S.S.   (4)

2.375

SHALLOW HEAD SHOULDER SCREW
STOCK DRIVE PRODUCTS
#7YS-CF5   (4)

FRONT VIEW
COVER PLATES REMOVED

RIGHT SIDE VIEW
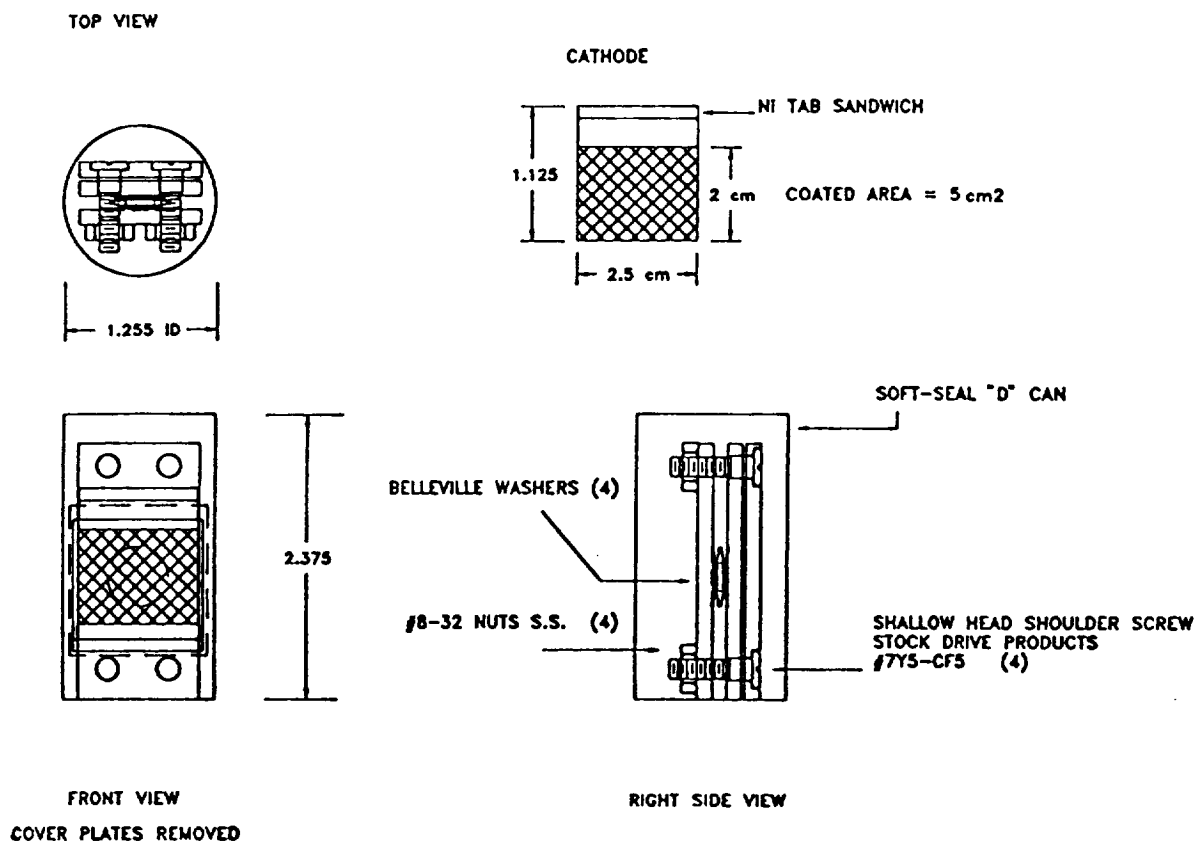
Fig. 41. Schematic of a cell used to apply specific, constant pressure (200 psi) to a parallel prismatic plate electrode stack.

45
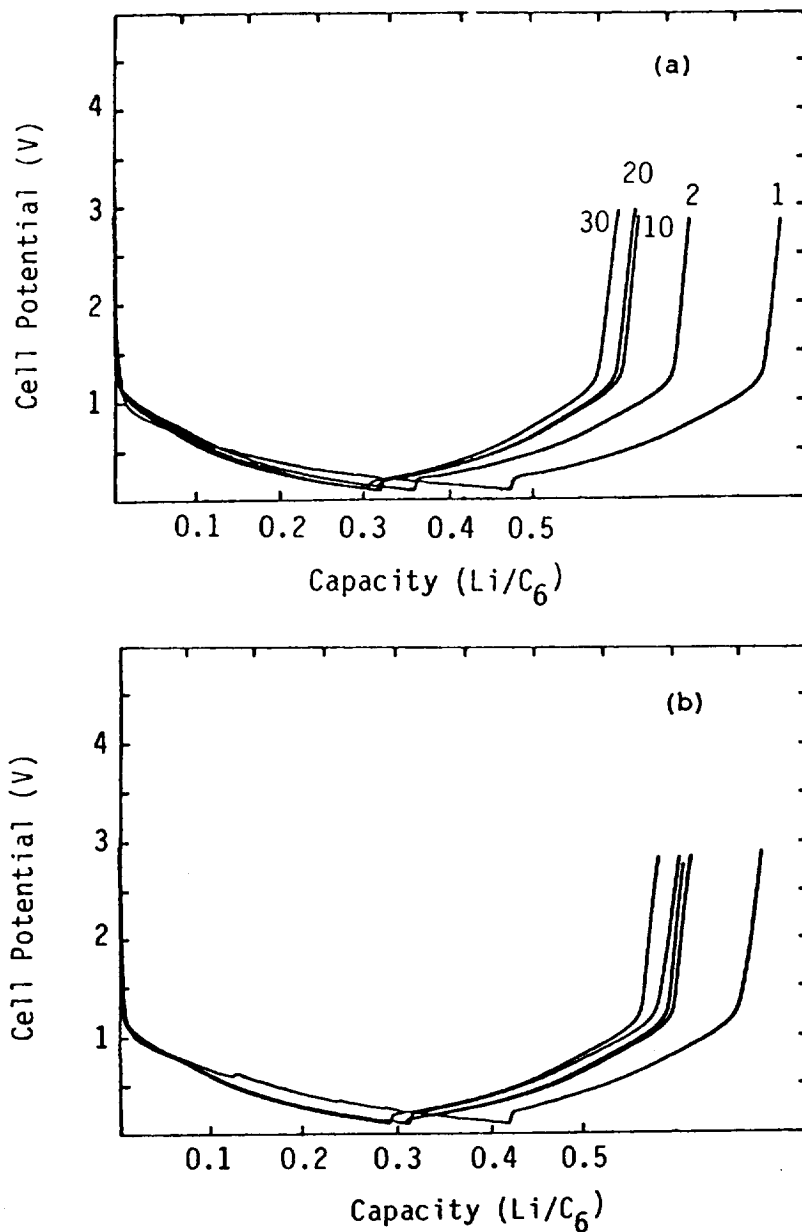
Fig. 42. Cycling curves for Li/C cells in which the carbon electrode was prepared from Conoco 5-6 μm petroleum coke. For (a) the carbon electrode measured 2.54 cm x 3.81 cm x 0.015 cm; for (b) the electrode was 5 cm x 5 cm x 0.012 cm and a stack pressure of 200 psi was applied. The electrolyte was PC/1.0M LiClO$_4$, and the current density was ±0.1 mA/cm^2.
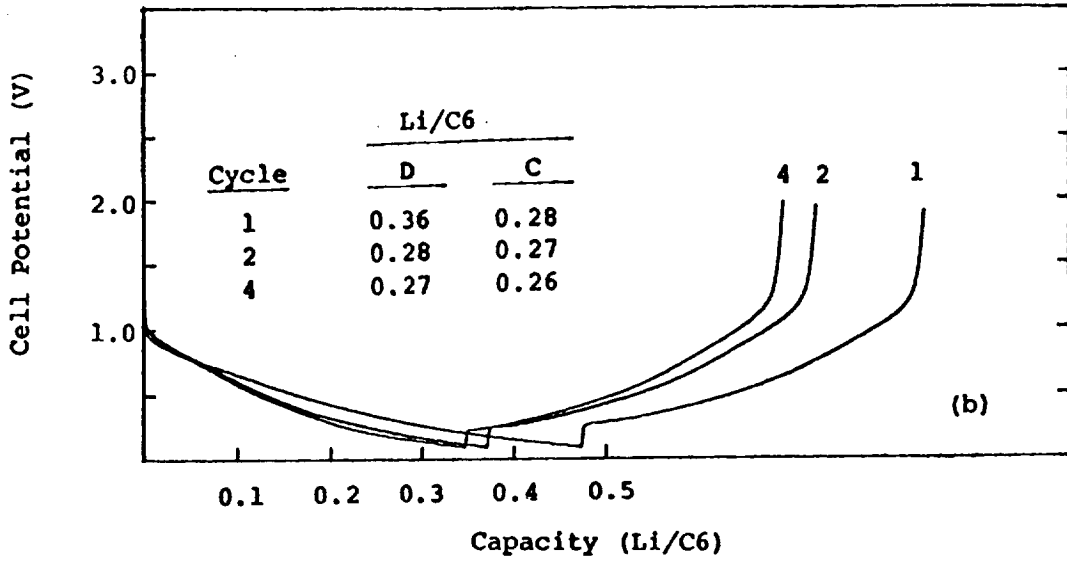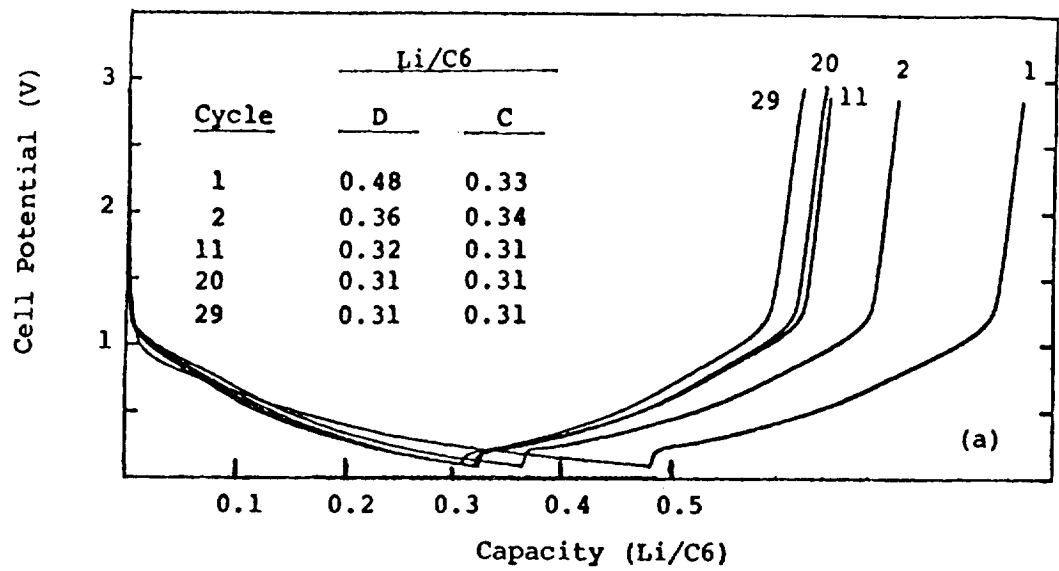
Fig. 43. Typical cycling curves for Li/C cells containing (a) Conoco 5 μm and (b) Conoco 75 μm petroleum coke. The electrolyte was PC/1.0M LiClO₄, and the current density was 0.1 mA/cm².

cells appears to be comparable, with somewhat better capacity retention than the earlier cells prepared using pasted electrodes. The cell with our regular configuration has an initial capacity of 0.48 Li/C_6 and a capacity of 0.31 Li/C_6 after 30 cycles. With respect to first-cycle discharge capacity, the cell with an applied stack pressure of 200 psi had a capacity of 0.42 Li/C_6, and the capacity was 0.30 Li/C_6 after 24 cycles. Figure 42 shows typical cycling curves obtained with each cell, and the capacity is normalized and expressed as Li/C_6. Apparently stack pressure is not an important variable for improving the performance of these electrodes.

The continuous cycling of these cells was interrupted to perform a rate capacity study. The data, summarized in Table 9, show that the only consistent improvement is at the 0.4 and 0.5 mA/cm^2 rate, where the capacity is 16 to 20% greater in the cell with the 200 psi stack pressure. At the end of the rate/capacity study the cells were cycled at the 0.1 mA/cm^2 rate. When cycling was ended, 68 cycles had been obtained with the cell fabricated in the usual way and the last cycle capacity was 0.25 Li/C_6. The cell with the regulated stack pressure was cycled 42 times and the last cycle capacity as 0.3 Li/C_6.

Effect of Particle Size: We have extended this work to include Conoco petroleum coke of two different particle sizes. Figure 43a shows typical cycling curves obtained using the material having a 5 μm particle size, while the curves in Figure 43b were obtained with material having a particle size of approximately 75 μm. Cycling was performed at 0.1 mA/cm^2 and the electrolyte was 1.0M $LiClO_4$ in PC.

The first cycle capacity was 0.48 Li/C_6 in the case of the 5 μm particle size coke, and 0.36 Li/C_6 for the larger-particle material. At the second cycle the discharge capacity was 75% of the initial capacity (0.36 Li/C_6) for the 5 μm material and 78% of the first cycle discharge capacity (0.28 Li/C_6) for the carbon with 75 μm particles. These results imply that the smaller particle size is beneficial in terms of maximizing the overall discharge capacity. The second cycle discharge capacity is 75-78% of the initial capacity in both cases, and particle size does not seem to affect the gradual capacity fade rate. After 29 cycles the discharge capacity of the 5 μm material is nearly the same as that for the second cycle. Additional cycling tests are necessary to determine if the same is true for the 75 μm petroleum coke.

3.5.2 Graphite

Effect of Solvent and Acid Extraction on Graphite Structure: Graphite purification methods have involved extraction by organic solvents and mineral acids and it has been reported (11) that the immersion of natural graphite in HNO_3 causes the graphite to undergo an irreversible increase in volume. Since it is possible that such a volume increase will improve the reversibility of Li intercalation in graphite, we have subjected both natural and synthetic graphite samples to such purification procedures. Figure 44 shows a series of X-ray diffraction patterns obtained after various stages in the purification of the Madagascar graphite. In terms of the structural comparison, there

48
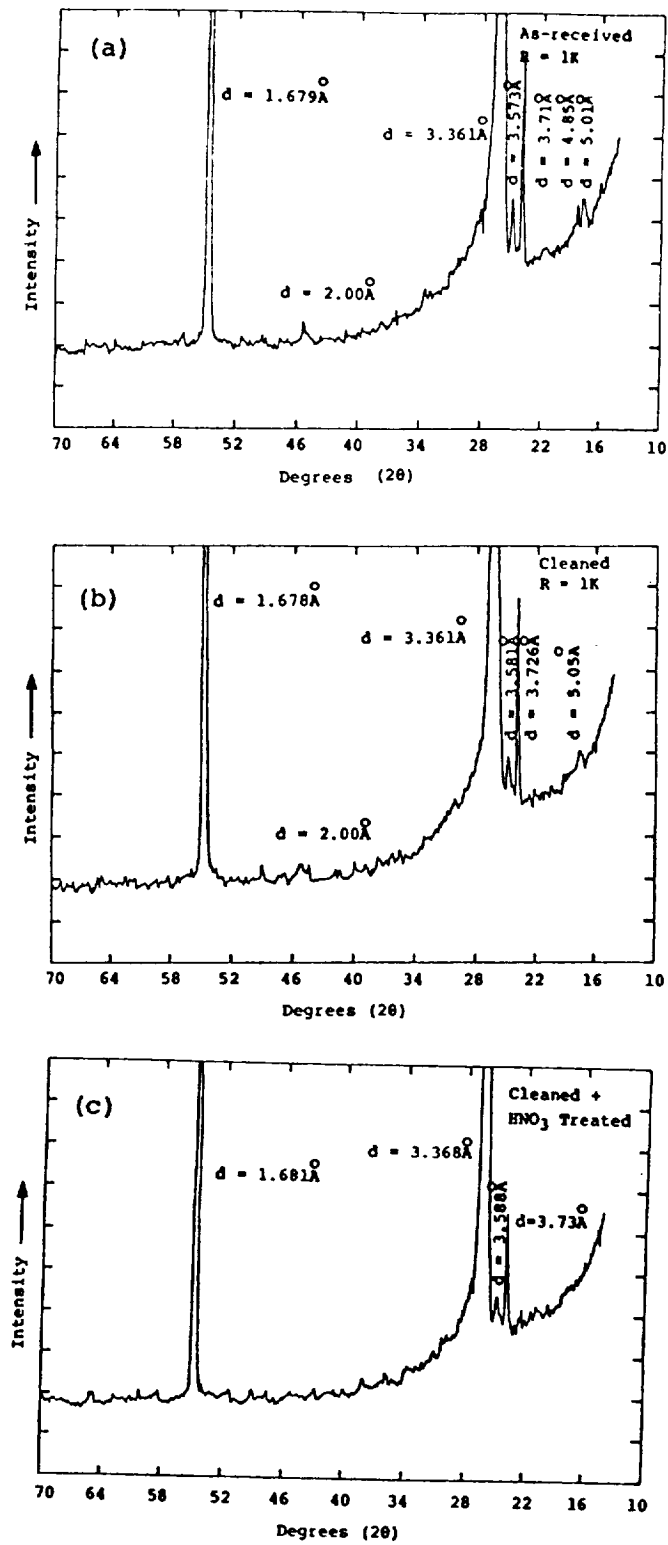
Fig. 44. X-ray diffraction patterns for Madagascar natural graphite (a) as received, (b) after extraction with toluene, and HCl and (c) after extraction with HNO₃.

Table 9. Rate/Capacity for Conoco, 5-6 μm.

Current Density (mA/cm^2)	Capacity (Li/C$_6$)	
	Standard Cell Configuration	200 psi Stack Pressure
0.05	0.33	0.308
0.1	0.30	0.30
0.2	0.26	0.27
0.3	0.25	0.24
0.4	0.19	0.22
0.5	0.20	0.25

appears to be a gradual removal of diffraction lines with d-space values of 4-5Å. This is evident from close comparison of the X-ray patterns for the graphite as-received (Fig. 44a), the graphite after extraction with toluene followed by extraction with HCl (Fig. 44b), and finally, after extraction with HNO$_3$ (Fig. 44c). Natural graphites from China and Zimbabwe which were subjected to the same procedures yielded the same results. Diffraction lines with d-space values of 3.37Å and 1.68Å correspond to the (002) and (004) reflections. Diffraction lines with d-space values greater than approximately 3.4Å are probably attributable to impurity phases, since they are not present in the ASTM reference X-ray patterns for graphite.

The synthetic graphite was treated the same way except that the extraction with HNO$_3$ was omitted since this had been reported to have no effect upon synthetic graphite. The X-ray diffraction patterns of this material (Fig. 45) show the two strong diffraction lines attributable to the (002) and (004) planes, and a low intensity peak with a d-space of 3.738Å. The cleaning process does not seem to have altered the structure of the synthetic graphite.

It appears that the cleaning resulted in only minor structural changes in the natural graphite samples and that the single synthetic graphite sample was unchanged. Cycling results obtained with these "cleaned" graphite samples were identical to those obtained with graphite not subjected to these procedures. In each case an irreversible reaction, probably electrolyte reduction, occurred at approximately 1V.

3.6 Evaluation of Alternate Electrolyte Salt

Selection of the electrolyte salt is crucial to the overall safety concerns involving Li batteries. LiClO$_4$, while possessing good electrochemical properties, is dangerous because of its strong oxidizing ability. Similarly, LiAsF$_6$ can be used to prepare highly conductive solutions, however,
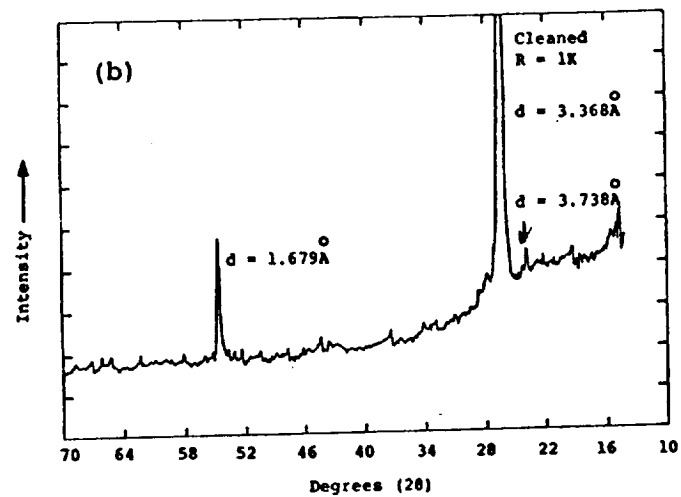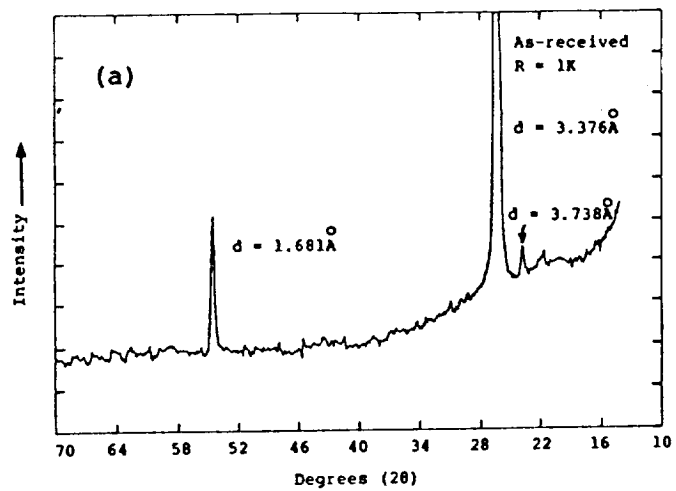
Fig. 45. X-ray diffraction patterns for Asbury A625 synthetic graphite (a) as received, and (b) after extraction with toluene and HCl.

51

the presence of arsenic poses a significant health and environmental hazard in the event of cell leakage or rupture. For these reasons, we tested lithium trifluoromethanesulfonimide $(LiN(CF_3SO_2)_2)$ as an alternative salt.

Figure 46 shows the results of conductivity measurements made for solutions of this salt prepared using the a) THF:2-MeTHF:2-MeF or b) the more viscous EC:PC:Triglyme solvent mixture. For the solution containing the ether mixture, the maximum conductivity at room temperature is 6.26 x $10^{-3}\Omega^{-1}cm^{-1}$ for the 1.2M salt concentration. When $LiAsF_6$ is used (3) the maximum conductivity is obtained when the salt concentration is 1.5M, and is nearly double (10.5 x $10^{-3}\Omega^{-1}cm^{-1}$). The viscosity of the EC:PC:Triglyme mixture severely limits the solubility of the salt and the conductivity of the solution. The 1.0M solution represents the upper solubility limit at room temperature, and at this concentration the conductivity is maximized at temperatures from -10°C through 70°C. The role of viscosity in determining the conductivity is apparent when one considers the results obtained with this particular solution. At room temperature the conductivity is 6.69 x $10^{-3}\Omega^{-1}cm^{-1}$. When the temperature is increased to 70°C the conductivity is more than doubled to a value of 15.0 x $10^{-3}\Omega^{-1}cm^{-1}$, while chilling to -10°C reduces the conductivity by a factor of three to 2.20 x $10^{-3}\Omega^{-1}cm^{-1}$. For the ether based solution, a change in temperature from 20°C to 70°C increased the conductivity by just 14%, while cooling to -20°C causes the conductivity to drop by just 32%.

Figures 47 through 49 show typical cycling curves for several cells. The cells represented by Figures 47 and 48 contained the THF:2-MeTHF:2-MeF\LiN(CF_3SO_2)_2 electrolyte, while the cell represented by Figure 49 contained the PC:EC:Triglyme\LiN(CF_3SO_2)_2 electrolyte.

In the case of the cells containing the ethers as solvent, the anode was either lithium (Fig. 47) or 70 LiAl (Fig. 48), and the cathode was TiS_2. Cycling was performed at 1 mA/cm², and plateaus observed in the charge portion of some of the cycling curves indicated that both cells were shorting. Cycle life of these cells was limited, and the FOM_{Li} was approximately 3 for both cells.

The first three cycles of the 70 LiAl/TiS_2 cell containing the EC:PC:Triglyme\ $LiN(CF_3SO_2)_2$ electrolyte (Fig. 49) were performed at 0.25 mA/cm². This current density was selected as a result of our previous experience with these solvents which seemed to indicate that initial cycling at a low rate is necessary to clean passivating films from the anode surface. Subsequent cycling was done using a current density of 1.0 mA/cm². This cell had an FOM_{Li} of 13.3 which is equivalent to a Li cycling efficiency of 92.5%.

52
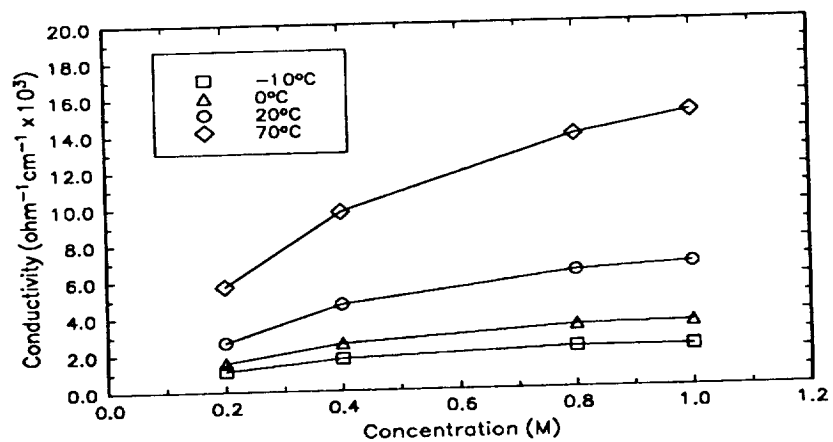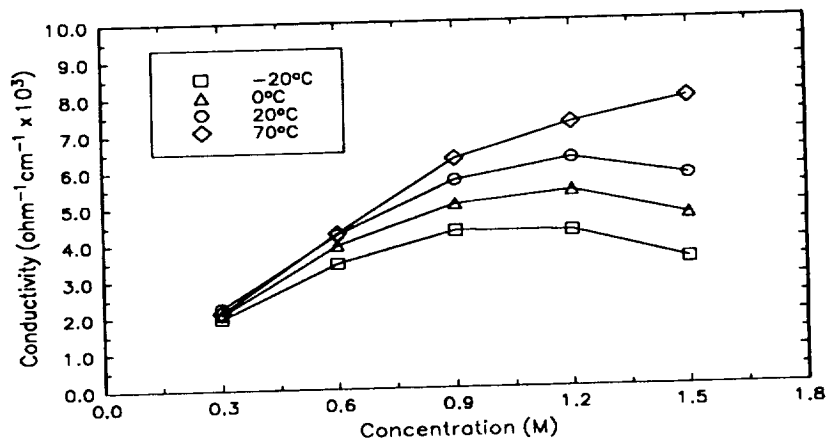
Fig. 46. Conductivity data for lithium trifluorosulfonimide solutions prepared with solvent mixtures of (a) 48 v/o THF:48 v/o 2-MeTHF:4 v/o 2-MeF, and (b) 35 v/o EC:35 v/o PC:30 v/o triglyme.
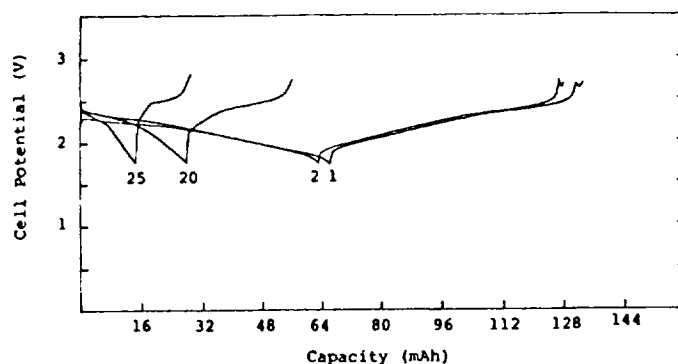
Fig. 47. Cycling curves for a Li/TiS$_2$ cell containing the 48 v/o THF:48 v/o 2-MeTHF:4 v/o 2-MeF\1.2M LiN(CF$_3$SO$_2$)$_2$ electrolyte. Theoretical capacity was 60 mAh and the current density was 1 mA/cm^2.
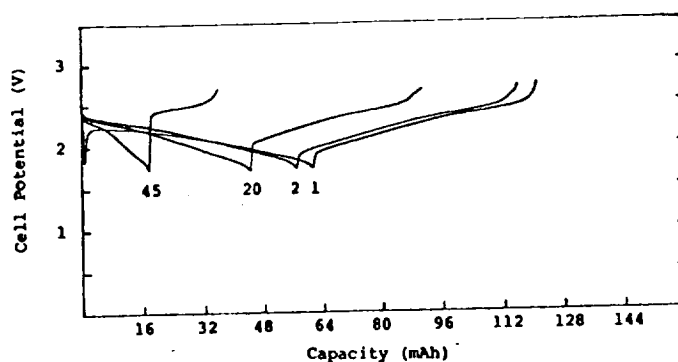
Fig. 48. Cycling curves for a 70 LiAl/TiS$_2$ cell containing the 48 v/o THF:48 v/o 2-MeTHF:4 v/o 2-MeF\1.2M LiN(CF$_3$SO$_2$)$_2$ electrolyte. Theoretical capacity was 60 mAh and the current density was 1 mA/cm^2.
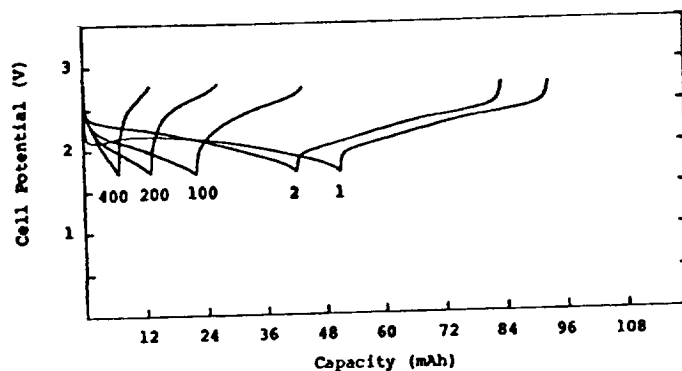
Fig. 49. Cycling curves for a 70 LiAl/TiS$_2$ cell containing the 35 v/o EC:35 v/o PC:30 v/o Triglyme\1.2M LiN(CF$_3$SO$_2$)$_2$ electrolyte. Theoretical capacity was 60 mAh. The current density was 0.25 mA/cm^2 for the first three cycles and 1.0 mA/cm^2 for the rest.

54

In terms of cycling performance, it is difficult to conclude on the basis of these few cells that the $LiN(CF_3SO_2)_2$ salt is responsible for the poor Li cycling efficiencies obtained with Li/TiS_2 and 70 $LiAl/TiS_2$ cells containing the $THF:2\text{-}MeTHF:2\text{-}MeF\backslash LiN(CF_3SO_2)_2$ electrolyte, since the poor cycling performance of these two cells may be due to mechanical rather than chemical causes. This is especially true in light of the results obtained with the $PC:EC:Triglyme$ based electrolyte, since the Li cycling efficiency of the cell containing this electrolyte was 92.5%, and this result was close to the 94.2% efficiency we reported previously for a similar cell in which the salt was $LiAsF_6$.

The fact that the Li cycling efficiency of the relatively viscous $PC:EC:Triglyme\backslash LiN(CF_3SO_2)_2$ mixture is nearly the same as that obtained with $PC:EC:Triglyme\backslash LiAsF_6$ suggests that $LiN(CF_3SO_2)_2$ is a suitable substitute for $LiAsF_6$. In the event that the Li cycling efficiency in the $THF:2\text{-}MeTHF:2\text{-}MeF\backslash LiN(CF_3SO_2)_2$ electrolyte is better than the present results indicate, it will allow for more complete replacement of $LiAsF_6$ by $LiN(CF_3SO_2)_2$. The fact that conductivities of solutions containing $LiN(CF_3SO_2)_2$ are lower than those containing $LiAsF_6$ will limit the use of the imide salt to applications which do not require high rates.

4.0 SUMMARY AND CONCLUSIONS

The work conducted during the course of this program served to evaluate anode materials and other cell components of secondary Li batteries in terms of their relative contributions toward the practical safety of such cells. The ultimate goal was the identification of factors which might contribute to safety problems and possible corrective actions necessary to the development of long-lived secondary Li batteries. Proposed improvements were the use of δ-LiAl alloy or carbon anodes, and lithium trifluormethanesulfonimide, an arsenic free salt.

The initial phase of the work focused on the investigation of the use of δ-LiAl alloys as alternatives to pure Li foil anodes. The exploratory study (1) indicated that these alloys could offer significant safety advantages without much sacrifice of cell performance. The improved safety would result from the reduction in the net amount of Li present in an anode of any particular volume.

Experiments were conducted using δ-LiAl alloy compositions with 60-85 w/o Li. X-ray diffraction analysis was used to show that these materials are two-phase mixtures containing elemental Li and a phase with the stoichiometry Al_4Li_9. Li cycling efficiency studies were performed using four alloy compositions (60 LiAl, 70 LiAl, 80 LiAl, and 85 LiAl) in laboratory cells at both 25% and 100% depths of discharge. Three electrolytes were used for these tests. Two (48 v/o THF:48 v/o 2-MeTHF:4 v/o 2-MeF/LiAsF$_6$ (1.5M) and 48 v/o 2-MeTHF:28 v/o Diox:20 v/o THF:4 v/o 2-MeF/LiAsF$_6$ (1.5M)) are ether-based, while the third (35 v/o PC:35 v/o EC:30 v/o triglyme/LiAsF$_6$ (1.0M)) contains mostly cyclic esters.

The Li cycling efficiency was calculated using the amount of free or elemental Li in each anode as the amount of lithium available for cycling. This made it possible to correlate the results of the Li cycling experiments with the anode composition. Whereas laboratory Li/TiS$_2$ cells cycle lithium with an efficiency of 96-97.5% in the standard binary electrolyte, practical AA Li/TiS$_2$ cells developed at EIC have a cycle life of 250 cycles and an average Li cycling efficiency of 99% with the same electrolyte. For all the δ-LiAl/TiS$_2$ laboratory cells tested in this program the lithium cycling efficiency was between 94.0 and 96.7%, regardless of alloy or electrolyte type.

A larger number of cell tests are necessary to determine the statistical significance of the small differences in cycling efficiency which occurred for the laboratory cells tested during the course of this work. The alloy with the best apparent performance depended upon the electrolyte selected and the discharge depth. In the case of the standard electrolyte, the 70 LiAl anode had the highest (96.4%) cycling efficiency, and this was at the 100% discharge depth. Cycling results obtained with the ternary electrolyte containing dioxolane showed a cell with the 85 LiAl alloy to have the highest cycling efficiency (96.4%) at the cycling depth of 25%. This data set underscores the difficulty of selecting a single 'best' alloy, since a cell with the 60 LiAl alloy cycled under the same conditions yielded an efficiency of 96.2%. These results do not appear to adequately reflect the

56

large difference in composition for these two alloys. We found that the discharge capacity of cells containing the 35 v/o PC:35 v/o EC:30 v/o triglyme/LiAsF$_6$ (1.0M) electrolyte increased gradually with continued cycling, and in some instances it was necessary to perform the initial cycling at a low (0.25 mA/cm^2) rate. It appears that this electrolyte passivates the surface of the anode much more severely and the passivation layer must be disrupted before the cells can be cycled. In this instance, the clearly best performer was the cell with the 60 LiAl anode that was cycled at a 25% d.o.d. yielding an efficiency of 96.7%. This was the highest lithium cycling efficiency for any of the laboratory cells tested in this program.

Overall, it appeared that the 60 LiAl alloy could be used for further tests in AA-size practical cells without much sacrifice of cycling efficiency compared to pure Li. This alloy is not malleable enough to use in a spirally wound electrode configuration, however, so that AA cell studies were performed using 70 LiAl as the anode. The relatively close cycling efficiency results indicated that this was not an inordinate compromise.

Testing of AA cells included capacity/rate studies and abuse testing by shorting or heating cells after a brief cycling period. The theoretical capacity of the 70 LiAl/TiS$_2$ cells was 700 mAh, and capacity/rate tests were performed at rates of 0.75 mA/cm^2 through 5 mA/cm^2. Cells tested this way had either the standard electrolyte or the one containing dioxolane. When the 0.75 mA/cm^2 rate was used the capacity was 680 mAh in both instances. For the 5 mA/cm^2 rate the cell containing the standard electrolyte yielded 600 mAh while the one containing the alternate electrolyte yielded 567 mAh. Although Li/TiS$_2$ cells containing the standard electrolyte have an average cycling efficiency of 99%, a lower cycling efficiency was observed in the 70 LiAl/TiS$_2$ cells tested with these two ether-based electrolytes. In the case of the standard electrolyte the Li cycling efficiency was 95.8%, while the cell containing the dioxolane-modified electrolyte had an efficiency of 94.3%. These results also indicate that the use of the 70 LiAl alloy does not significantly limit the rate capability, although there is a significant loss of lithium cycling efficiency compared to similar cells having lithium anodes.

We have found that heating cells is a good way to mimic the failure of a cell by the development of a 'soft' short during cycling. Experiments performed with either the Li/TiS$_2$ or 70 LiAl/TiS$_2$ couple, and the standard electrolyte resulted in a drop in the OCV when the external cell temperature was well below the melting point of lithium. In both cases an exotherm at 150°C coincided with the cell voltage dropping to zero. Direct shorting of cells which had been cycled five times generated external cell temperatures of 93°C or 106°C when the 48 v/o 2-MeTHF:28 v/o Dioxolane:20 v/o THF:4 v/o 2-MeF/LiAsF$_6$ (1.5M) electrolyte was used with a 70 LiAl/TiS$_2$ or Li/TiS$_2$ couple. (The current generated by shorting was 8.9A for the former and 13.5A for the latter). The heated cells ruptured at the point where the cover was welded to the can, while the shorted cells remained intact. The use of the δ-LiAl alloy does not appear to greatly improve the cell's ability to withstand heating or direct shorts.

The second major effort of our program was the used of Differential Scanning Calorimetry to look for relationships between the various cell components and the thermal flux of the cell when it is heated. One unanticipated result of this study was the finding that the binary electrolyte (48 v/o THF:48 v/o 2-MeTHF:4 v/o 2-MeF/LiAsF$_6$ (1.5M)) underwent a significant exothermic reaction when heated, and that much of this heat was evolved at or below the melting point of the Celgard separator (~160°C). A heat contribution from the cell components would mean that the separator could melt before the external cell temperature reached 160°C. Examination of reactions between the three solvents that are used to prepare this electrolyte and LiAsF$_6$ indicates that THF and 2-MeTHF both undergo exothermic reactions, but that the one involving 2-MeTHF is the larger of the two when the results are normalized to account for the sample mass. The additive 2-MeF does not show any significant reaction under the same conditions.

The ternary electrolyte containing dioxolane is similar in composition to the binary electrolyte and has a similar DSC scan. Triglyme, used with the cyclic esters to prepare another ternary electrolyte has a 3.5 W/g exotherm at about 250°C. This seems to have little influence on the DSC scan of the ternary electrolyte where it is present as 30v/o, and this electrolyte does not evolve much heat.

Experiments performed with electrolytes in contact with fresh Li foil show that the predominant exothermic reaction occurs below the melting point of lithium when the electrolytes contain ethers, and that the exotherms correspond to those seen when the electrolytes alone are tested. Experiments with Li and EC, PC or the ternary electrolyte containing triglyme do not show evidence of any significant exothermic reaction attributable to the presence of lithium.

DSC experiments performed with wet anode materials removed from cycled cells show that the presence of high surface area lithium guarantees that all the electrolytes which we used will undergo an exothermic reaction. The exotherm starts at about 100°C when the electrolytes contain ethers, and the ones containing the esters start to react at a temperature as low as 50°C. These findings mean that the melting of elemental lithium is not necessary for significant exothermic reaction to be initiated when a cycled cell is heated. Experiments using wet cathode materials removed from cycled cells after charge (to lessen the possible presence of elemental lithium) showed exotherms starting at about 100°C. This indicates that even the cathode, stripped of any elemental lithium, may contribute to the exotherms obtained when cycled cells are heated.

The concept that cell safety could be improved readily by limiting or eliminating elemental lithium from the cell led us to undertake some preliminary studies with carbon anodes. For these experiments we used carbon from several commercial and natural sources. These materials included both the poorly ordered 'petroleum cokes' and natural and synthetic graphite. Experiments with the petroleum cokes showed that for a particular type and size carbon, capacity and capacity retention were the same whether we used our regular laboratory cell configuration or a specific (200 psi) constant stack pressure. With respect to particle size, Conoco petroleum coke with a 5μm size had a higher initial capacity (0.48 Li/C$_6$) than the same material with 75μm particles, but the capacity

fade rate was about the same in both cases with the second cycle providing 75-78% of the first discharge capacity. Graphite samples were fabricated into electrodes in the same manner as the petroleum cokes, but could not be cycled. The same result was obtained whether the material was natural or synthetic in origin, and whether or not it had been extracted with toluene and acid to remove soluble impurities.

Further safety improvements involve the replacement of $LiAsF_6$ as the electrolyte salt. Besides eliminating arsenic as a toxicity hazard, it may result in elimination of the exothermic solvent/salt reactions which were described above. With these points in mind, a brief study of electrolytes prepared with the 48 v/o THF:48 v/o 2-MeTHF:4 v/o 2-MeF or 35 v/o EC:35 v/o PC:30 v/o Triglyme solvent mixtures and the $LiN(CF_3SO_2)_2$ salt was performed. The maximum conductivity obtained with the imide salt in the ether mixture was $6.26 \times 10^{-3} \, \Omega^{-1}$-$cm^{-1}$ at room temperature. This is roughly half the conductivity obtained at room temperature with the standard binary electrolyte containing $LiAsF_6$. A 1.0M concentration of $LiN(CF_3SO_2)_2$ in the other ternary solvent mixture yields a maximum conductivity of $6.69 \times 10^{-3} \, \Omega^{-1}$-$cm^{-1}$. Only limited cycle life studies were performed, but it appears that the lower conductivity may be tolerable for cells meant for low-rate applications.

5.0 REFERENCES

1. K. M. Abraham, M. Alamgir, and E. Willstaedt, Final Report for Contract No. NAS7-1042, August 22, 1989.

2. K. M. Abraham, P. B. Harris, and D. L. Natwig, J. Electrochem. soc., 130, 2309 (1983).

3. K. M. Abraham, D. M. Pasquariello, and F. J. Martin, J. Electrochem. Soc., 133, 661 (1986).

4. A. C. Makrides, K. M. Abraham, G. L. Holleck, T. H. Nguyen, and R. J. Hurd in 34th International Power Sources Symposium, p. 167, (1990).

5. K. M. Abraham and S. B. Brummer, Chapter 14 in Lithium Batteries, J. P. Gabano, Editor, Academic Press, NY (1983).

6. V. R. Koch, J. Power Sources, 6, 357 (1981).

7. J. O. Besenhard and G. Eichinger, J. Electroanal. Chem. Interfacial Electrochem., 68, 1 (1976).

8. J. O. Besenhard, P. Komenda, A. Paxinos, and E. Wudy, Solid State Ionics, 18, 823 (1986).

9. Celgard microporous film technical information circular, Celanese Corp., Charlotte, N.C.

10. U. von Sacken, and J. R. Dahn, Abstract No. 54, p. 87 in Extended Abstracts of the Fall Meeting of The Electrochemical Society, Seattle, WA, October 14-19 (1990).

11. C. L. Mantell, Carbon and Graphite Handbook, Interscience Publishers, NY (1968).

1. Report No.	2. Government Accession No.	3. Recipient's Catalog No.
4. Title and Subtitle Long Cycle Life Rechargeable Lithium Batteries		5. Report Date October 19, 1992
		6. Performing Organization Code
7. Author(s) D. M. Pasquariello, W. B. Willstaedt and K. M. Abraham		8. Performing Organization Report No. 89063
		10. Work Unit No.
9. Performing Organization Name and Address EIC Laboratories, Inc. 111 Downey Street Norwood, Massachusetts 02062		11. Contract or Grant No. NAS7-1100
		13. Type of Report and Period Covered
12. Sponsoring Agency Name and Address National Aeronautics & Space Administration Jet Propulsion Laboratory 4800 Oak Grove Drive Pasadena, California 91109		14. Sponsoring Agency Code Final Report 04/23/90 - 10/20/92
15. Supplementary Notes		

16. Abstract

Cycle life and safety of δ-LiAl/TiS$_2$ cells were evaluated using laboratory and AA-size cells. Analysis of the alloys (which contained 60, 70, 80, or 85 weight-percent lithium and are designated 60 LiAl etc.) showed them to contain a mixture of elemental Li and Al$_4$Li$_9$. Cycling efficiencies correlated with the amount of free lithium in the anode. Using an electrolyte with the composition 48 v/o THF:48 v/o 2-MeTHF:4 v/o 2-MeF/LiAsF$_6$ (1.5M), a 70 LiAl/TiS$_2$ laboratory cell yielded a cycling efficiency of 96.4% when cycled at a 100% discharge depth which compares well with Li anode cycling efficiencies of 96-97.5% obtained previously in this electrolyte. The highest cycling efficiency of any δ-LiAl/TiS$_2$ laboratory cell was 96.7% when the 60 LiAl alloy was used with the 35 v/o PC:35 v/o EC:30 v/o triglyme/LiAsF$_6$ (1.0M) electrolyte. The 70 LiAl alloy was selected for further testing in AA cells since it was malleable for the fabrication of spirally wound electrodes, and its overall cycling performance was sufficiently good.

AA-size 70 LiAl/TiS$_2$ cells appear to have capacity/rate properties similar to those for identical Li/TiS$_2$ cells. The use of the δ-LiAl alloy anodes does not appear to offer any safety advantage when cycled cells are shorted or heated.

17. Key Words (Suggested by Author(s)) Rechargeable lithium batteries, alloy anodes	18. Distribution Statement Limited distribution to NASA personnel.	
19. Security Classif. (of this report)	20. Security Classif. (of this page)	21. No. of pages 69	22. Price

16. Abstract (continued)

Differential Scanning Calorimetry studies conducted with the various cell components and with material removed from electrodes after cycling show that the electrolyte can be a significant contributor to the thermal instability of a secondary Li cell. In particular it was found that THF and 2-MeTHF undergo strongly exothermic reactions when they contain $LiAsF_6$ as a solute and are heated. These exotherms occur at about 170°C when the single solvents are used, but in the mixed electrolyte the exotherm covers the 150°C-200°C temperature range. These reactions appear capable of contributing heat for the melting of the polypropylene separator at 160°C and lithium at 180°C.

Alternate anodes which are lithium intercalated carbon were also studied in which the carbon was either petroleum coke or graphite. Conoco petroleum coke with a 5 μm particle size had the best capacity (0.48 Li/C_6) but 28% of this capacity was irrecoverable. A steady capacity fade was observed and after 20 cycles the capacity was approximately 0.3 LiF/C_6. No graphite samples cycled Li reversibly, even after attempts were made to remove soluble organic and inorganic impurities.

It is desirable to eliminate the use of arsenic in the cell and for this reason lithium trifluorosulfonimide was used to prepare a series of ether and ester-based electrolytes. The room temperature conductivity of a mixed ether solution containing this salt is 6.26×10^{-3} Ω^{-1}-cm^{-1}, which is about half the conductivity of a similar electrolyte prepared with $LiAsF_6$. Preliminary cycling results indicate that this loss of conductivity may be tolerable for cell applications requiring low rates.